ARTICLES

Solvation Ultrafast Dynamics of Reactions. 11. Dissociation and Caging Dynamics in the Gas-to-Liquid Transition Region

Christoph Lienau[†] and Ahmed H. Zewail*

Arthur Amos Noyes Laboratory of Chemical Physics, California Institute of Technology, Pasadena, California 91125

Received: August 9, 1996[⊗]

In this paper we give a full account of the work presented in earlier communications [Lienau et al. *Chem. Phys. Lett.* **1993**, *213*, 289; **1994**, *218***,** 224; *J. Chim. Phys.* **1995**, *92***,** 566]. With femtosecond time resolution, studies are presented of the dynamics in real time of an elementary chemical reaction, the dissociation and recombination of iodine in supercritical rare-gas solvents, in the gas-to-liquid transition region. Through pressure variation, the properties of the solvent, helium, neon, argon, or krypton, are changed from those of an essentially ideal gas at low densities to those of a liquidlike fluid at pressures of several thousand bar. Of particular interest here are (i) the impact of solute−solvent interactions on the coherence of the wave packet nuclear motion, (ii) the collision-induced predissociation of the B state, and (iii) the geminate recombination of the atomic fragments and the subsequent vibrational energy relaxation within the A/A′ states. In helium and neon, the coherence of the vibrational motion persists for many picoseconds, even at pressures of 2000 bar. For pressures between 100 and 2000 bar of helium and neon, the dephasing rate is only weakly affected by the solvent density. In all solvents, the solvent-induced predissociation rate increases nearly linearly with solvent density. In argon at 2500 bar, the predissociation rate reaches 1.05 ps^{-1}. Relative geminate recombination yields for the formation of new A/A′ state iodine molecules and the time scale for the geminate recombination and the subsequent A/A′ state vibrational relaxation dynamics are also studied. The solvation and chemical dynamics are examined, using simple analytical models, in relation to the solvent density and polarizability. With the help of molecular dynamics, detailed in the accompanying paper, we present a microscopic picture of the elementary processes under the free and solvation conditions encompassing the different density regimes in the gas-to-liquid transition region.

I. Introduction

The microscopic description of chemical reactions in solutions involves many-body interactions. These solute−solvent interactions may induce changes in the potential energy surface governing the dynamics of the isolated gas-phase system but certainly will influence the reaction trajectories on the time scale of the collision with the solvent. Even in the case of simple molecules, a precise mapping of the dynamics in liquid solutions is not an easy task.

In this series of papers, we focus attention on an approach designed to elucidate the real-time elementary dynamics of reactions in solutions. By examining the femtosecond dynamics at different solvent densities, up to the liquid-state density, we are able to follow the effect of solvation on reaction dynamics in a systematic way by varying solvent composition, type, or temperature. This requires changing the solvent pressure from 0 bar to, typically, 3000 bar. As indicated in our preliminary reports,[1−3] the approach offers unique opportunities for revealing the nuclear motions under "controlled" conditions of solvation. Initially, we have examined the rare-gas family of solvents. Variation of the rare-gas pressure allows us to study the reaction of interest in a solvent whose state changes from an essentially ideal gas at low pressures, through the gas-to-liquid transition region, to a liquidlike fluid at pressures of several thousand bar. Hence, the time between solute−solvent collisions is gradually brought to the time scale of the nuclear motion of the solvent, and we have an opportunity to study the elementary dynamics from the collision-free to the liquid-phase limit.

In this and the accompanying papers,[4] we give a full account of this approach and report studies of real-time dynamics of dissociation and recombination processes of a prototype diatomic molecule (iodine) in supercritical monatomic solvents. The same system has been studied in the cluster phase,[5] and the comparison allows us to examine the effect of "random" solvent structure. We have chosen iodine in supercritical rare-gas solvents (helium, neon, argon, and krypton) as a prototype system for a number of reasons. A wealth of information is available on the iodine system, both in the isolated gas phase and in solution. The gas-phase potential energy curves of the ground $X0_g^+(^1\Sigma)$ and excited $B0_u^+(^3\Pi)$ states are precisely known.[6] Moreover, the potentials of six of the nine excited electronic states that correlate with ground-state iodine atoms are experimentally known; these are the weakly bound $A'2_u(^3\Pi)$[7] and $A1_u(^3\Pi)$[8] and the repulsive $0_u^+(^3\Pi)$,[8] $a1_g(^3\Pi)$,[9,10] $B''1_u(^1\Pi)$,[9] and $a'0_g^+(^3\Sigma^-)$[11] states. This leaves only three of the ten Hund's case (c) states which correlate with ground-state iodine atoms, experimentally unknown. All of them are supposed to be repulsive. Rather extensive spectroscopic

[†] Deutsche Forschungsgemeinschaft Postdoctoral Fellow. Present address: Max-Born-Institut für Nichtlineare Optik und Kurzzeitspektroskopie, Rudower Chaussee 6, D-12489 Berlin, Germany.

[⊗] Abstract published in *Advance ACS Abstracts,* November 1, 1996.

S0022-3654(96)02430-6 CCC: $12.00

information is also available on 14 out of 20 ion-pair states of iodine, particularly those which are of interest here, *i.e.*, $D'2_g$,[8] $\beta 1_g$,[12] $D0_u^+$,[13] $E0_g^+$,[14] and $f0_g^+$.[15] This knowledge of potentials provides an excellent basis for a comparison of experimental findings to theoretical studies.

The second important feature of the system is the dynamics. The wave packet motions on the bound $B0_u^+(^3\Pi)$ state and on the $A1_u(^3\Pi)$ and $B''1_u(^1\Pi)$ states have been observed and studied on the femtosecond (fs) time scale.[16,17] The coherent nuclear motion in the B state persists for many picoseconds and reflects the period of the oscillation between the turning points of the potential. Careful analysis of the experimental results at different excitation wavelengths shows how information on potential energy surfaces can be extracted with precision.[18,19]

The fs dynamics in rare-gas solvents were first reported for iodine in argon.[20] At 100 bar, the motion of the wave packet was studied, and in these studies focus was on the effect of argon collisions on the vibrational coherences of the wave packet, the collision-induced B state predissociation, and the caging of iodine molecules excited above the B state dissociation threshold. Molecular dynamics simulations by Wilson's group were compared with the experimental findings to address the different time scales.[21] The experimental studies were further extended to argon densities in the gas-to-liquid transition region by Lienau et al.[1−3] They not only demonstrated the long persistence of coherent nuclear motion over more than 1.5 ps at pressures as high as 800 bar and the nearly linear increase of predissociation rate with density but also provided evidence for geminate recombination of dissociating iodine atoms onto the A/A′ states, a process which has been thoroughly studied for many years by nanosecond laser flash photolysis in the groups of Troe[22−26] and van den Bergh.[27,28] From accurate measurements of the quantum yields for geminate recombination (at long times) they have shown the dependence of the yield on pressure and solvent, and Troe's group advanced a diffusion model to account for these dependencies.[29]

In liquids, the photodissociation and recombination of iodine served as a prototype reaction for the "cage effect" since the early work of Franck and Rabinowitch in 1934.[30,31] The first experimental studies by Noyes,[32,33] Davidson,[34] and Porter[35] focused on the yield for geminate recombination of iodine and its dependence on the solvent viscosity.[36] Picosecond time-resolved studies of the dynamics of iodine started with Eisenthal's pioneering work on the ground-state recovery in CCl_4 and hexadecane.[37] From the transients they deduced a time scale for predissociation (∼10 ps) and related the long time behavior (∼100 ps) to the caging process. This work triggered theoretical and experimental studies in a number of research groups (Adelman, Bunker, Harris, Hopkins, Hynes, Kelley, Miller, Moore, Sceats, Wilson, and others). In 1982, Nesbitt and Hynes[38] reinvestigated the origin of the recovery time scale and pointed out the importance of slow ground-state vibrational relaxation, on the order of 100 ps, also discussed by Wilson and co-workers.[39] The interpretation is supported by molecular dynamics simulations[40−42] and was investigated by picosecond experiments in the groups of Kelley[43−45] and Wilson.[46,47] Moreover, Kelley's experiments showed that not only the ground X but also the excited A and A′ states are involved in the recombination process.

The progress that has been made in these solution-phase studies is summarized in the review article by Harris et al.[48] A detailed microscopic picture of the dissociation and recombination dynamics in solution emerged from a series of thorough picosecond studies in Harris' group.[49−53] From these studies it was concluded that the dissociation on the photoexcited B state

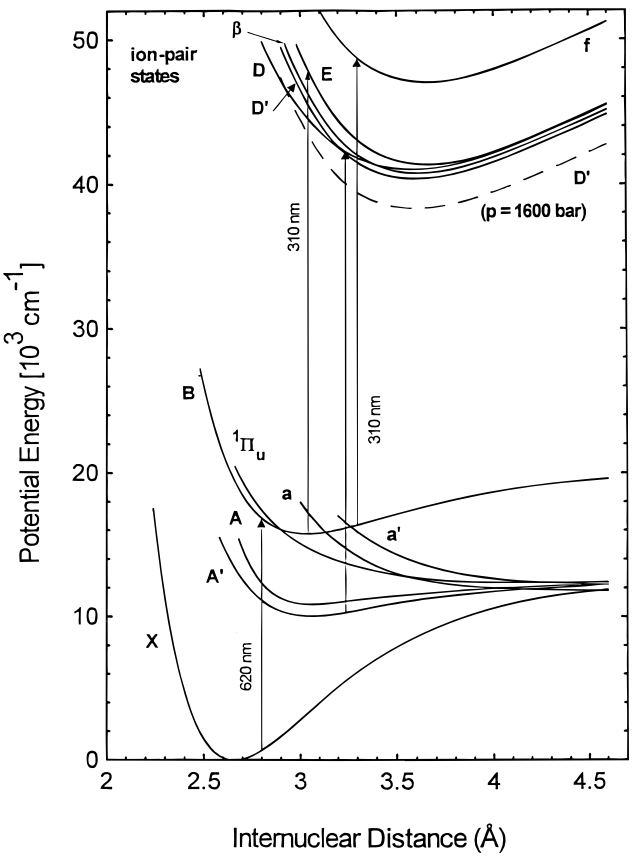

Figure 1. Potential energy curves of molecular iodine relevant for the present study. The dashed line indicates the solvent shift of the D′ ion-pair state in argon at 1600 bar and 293 K. The pump laser pulse prepares a wave packet on the quasi-bound $B0_u^+(^3\Pi)$ state (62%) or on the dissociative $A1_u(^3\Pi)$ (34%) or $B''1_u(^1\Pi)$ states. The B state dynamics is probed with a temporally delayed second pulse centered at 310 nm which can excite molecules near the outer turning point of the B state into the $E0_g^+$, or $f0_g^+$ ion-pair state. Fluorescence from the ion-pair states is detected as a function of the delay time between pump and probe pulses. With 310 nm probe pulses, A/A′ state molecules in low vibrational levels are probed, and the resulting ion-pair state fluorescence is detected. The wavelength of 310 nm is not sensitive to the probing of molecules in the high vibrational levels of the ground state. In the accompanying paper, the probe wavelength dependence is studied.

occurs in 2 ps or less and that the dissociating iodine atoms recombine on a similar time scale onto either the excited A/A′ or the ground X state (see Figure 1). New molecules formed on the ground state undergo vibrational relaxation on the time scale that has been predicted by Nesbitt and Hynes, and the vibrational relaxation dynamics could be characterized in a variety of solvents. Direct information on the ground-state vibrational relaxation was obtained from transient resonance Raman studies by Hopkins' group.[54] Subsequent to vibrational relaxation, molecules born on the excited A/A′ states undergo electronic curve crossing onto the ground state. A/A′ state lifetimes are strongly solvent dependent and range from 100 ps to 10 ns.[48] Studies of iodine in solution were made in the fs time regime by Scherer et al.[55,56] They reported that electronic B state predissociation in *n*-hexane occurs in ∼230 fs. Moreover, from their results they concluded that the dephasing time of the coherent B state vibrational wave packet motion is the same as the predissociation time. This dephasing time is in agreement with the findings of an earlier frequency domain, resonance Raman study by Sension and Strauss.[57] In liquid xenon and carbon tetrachloride, Schwentner and Chergui[58] have observed the progression of the I−I vibration and the incoherent

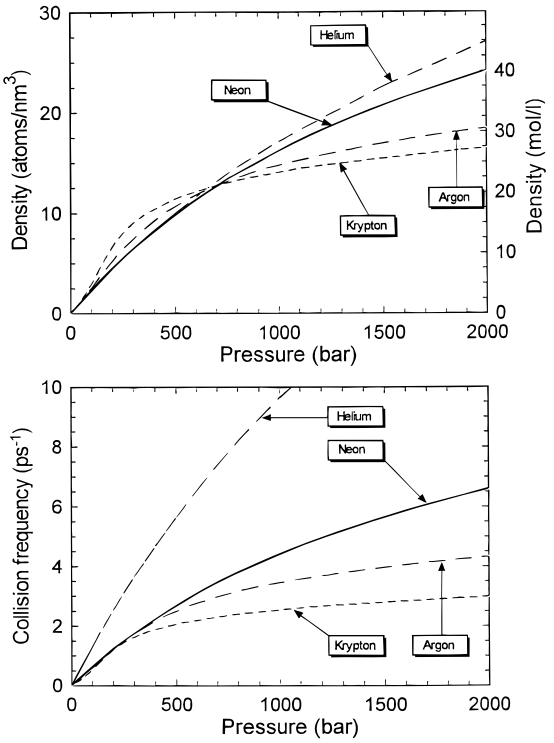

Figure 2. (top) Density of supercritical rare gases as a function of pressure at 293 K. For references to the experimental density values see the Appendix. (bottom) Pressure dependence of the hard-sphere collision frequency of iodine in the compressed rare gases helium, neon, argon, and krypton. Collision frequencies have been calculated using eq 17.

emission in the resonance Raman spectra and obtained a dynamical picture.

In the cluster phase, studies by Liu et al.[5,59] of the fs dynamics, which are of particular interest for the present work, have resolved the coherent dissociation and recombination processes of iodine encaged in large argon clusters. For excitation onto the A state, Liu et al. demonstrated an ultrafast coherent recombination within 600 fs. In such cold clusters, the iodine molecules are imprisoned inside a rigid solvent structure which is formed by the surrounding solvent atoms. The dynamics is therefore governed by a loss of vibrational energy to the surrounding solvent cage, and the quantum yield for geminate recombination is close to unity. The ultrafast coherent formation of new iodine molecules on either the A/A′ or the ground state is followed by a slower vibrational relaxation. It was pointed out[59] that the critical factors for observing such coherent motion in the solvent cage are the time scale for bond breakage and the rigidity of the solvent structure. These ideas were supported by MD calculations.[5] Indeed at lower temperatures in argon matrices, Apkarian's group[60] observed a persistent ultrafast coherent recombination. The coherent vibrational motion of the A state wave packet persists with its vibrational energy decreasing below the A state gas-phase dissociation energy. Martens, in a series of enlightening papers,[61,62] has given the theoretical foundation for this coherence in solids and pointed out the connections to the cluster phase.

In the present study, we focus on the dissociation and recombination dynamics of iodine (see potentials in Figure 1) in the supercritical rare-gas solvents (helium, neon, argon, and krypton) at pressures between 0 and 2000 bar. The variation of the solvent properties in this pressure range is displayed in the change of the macroscopic solvent density with pressure in Figure 2. While helium and neon follow approximately the linear "ideal-gas" relationship between density and pressure,

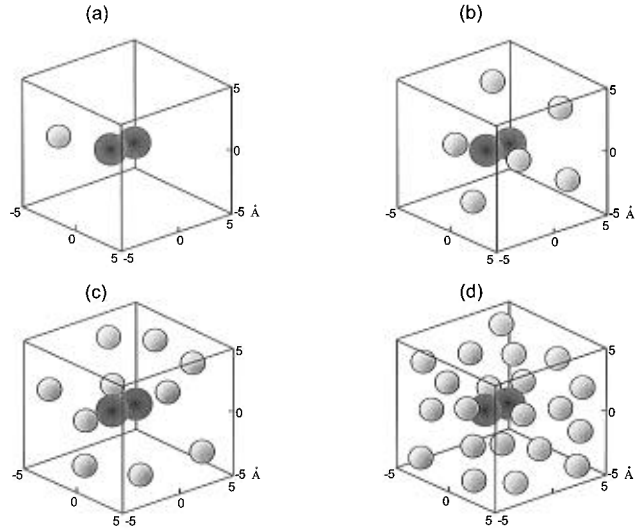

Figure 3. A schematic for the variation in solvent density with pressure for neon in the supercritical state. Accurate MD simulations are given in the accompanying paper.

especially at lower pressures, the pressure dependencies of argon and especially of krypton density show marked deviations from linearity. At pressures above 500 bar, the density of krypton increases only slightly with pressure, and therefore the compressibility of krypton decreases markedly. This reflects the closely packed structure of the krypton solvent at high pressures. In fact, the "packing fraction",[63] i.e., the amount of space occupied by the solvent atoms per unit volume, changes with solvent size and reaches, at a pressure of 2000 bar, 24% in helium and 27% in neon, compared to 38% in argon and 40% in krypton. A schematic of the change of the packing fraction with density is visualized in Figure 3. As shown in Figure 2, the iodine−solvent collision frequency,[64] in a simple hard-sphere model, varies with density, and at high pressures the time between collisions reaches the time scale of the nuclear iodine motion. We thus expect the iodine−solvent collisions to affect the dynamics on the fs time scale.

In order to study the pressure and solvent effect on the iodine fs dynamics, laser pulses with a duration of 60 fs were used to excite ground-state iodine molecules. At 620 nm, 62% of the excited molecules reach low vibrational levels $v' = 6-11$ of the bound $B0_u^+(^3\Pi)$ state[16] (centered around $v' = 8$), while 34% are placed on the weakly bound $A1_u(^3\Pi)$ state and the remainder on the dissociative $B''1_u(^1\Pi)$ state[65] (see Figure 1). The dynamics of the prepared wave packet are then interrogated by a second 60 fs, 310 nm pulse, which can excite B state molecules near the outer turning point of the B state into either the $f0_g^+$ [66,67] or $E0_g^+$ [68,69] ion-pair states of iodine. We detect the ion-pair state fluorescence as a function of the delay time between pump and probe pulses. This fluorescence is a measure of the B state population at the I_2 internuclear distances at which absorption can occur and allows us to monitor the dynamical evolution of this population. Ion-pair state fluorescence also originates from molecules in low vibrational levels of the $A'2_u$-$(^3\Pi)$ and $A1_u(^3\Pi)$, which are efficiently excited by the 310 nm probe pulses into either the $D'2_g$ or the $\beta 1_g$ state, as shown in Figure 1. Fluorescence induced by molecules in high vibrational levels on the ground state, however, will be shown to be negligible under our conditions.[4] Thus, these experiments are mainly sensitive to the coherent wave packet motion within the bound B state, the collision-induced B state predissociation, and a possible recombination of the dissociating atom pair onto the A/A′ states, followed by vibrational relaxation within these

states. The experiments are insensitive, however, to the dynamical evolution on the electronic ground state of iodine.

The paper is structured as follows. After a brief presentation of the experimental setup, we discuss the solvent and pressure effect on the ion-pair state fluorescence spectra and extract information on the solvent influence on the ion-pair state potentials. In the next section we discuss experimental results on the solvent-induced dephasing of the coherent vibrational wave packet motion. Pressure- and solvent-dependent rates for the collision-induced B state predissociation are compared to isolated binary collision models. In the final section, results on the yield and dynamics of the geminate atomic recombination are related to a diffusion-based model for the dynamics.

II. Experimental Section

The experimental setup has been described in detail elsewhere,[1] and only a brief summary follows (see also the accompanying paper). Laser pulses of 60 fs duration at a repetition rate of 100 MHz and a pulse energy of 20 pJ were generated from a home-built colliding-pulse mode-locked ring dye laser (CPM). These pulse were amplified to 1.5 mJ at a repetition rate of 30 Hz in a four-stage, Nd:YAG-pumped dye amplifier (PDA). The amplified pulses were temporally compressed in a double-pass, two-prism arrangement before being separated into pump and probe pulses by a 50/50 beam splitter. The pulse duration after compression was 60 fs. Together, the pump and probe lasers formed two arms of a Michelson interferometer. The probe laser was focused into a KD*P crystal to generate the 310 nm pulse, and the fundamental was removed with dichroic mirrors.

The pump and probe lasers were recombined with a dichroic beam splitter and then focused slightly beyond the center of the high-pressure cell to avoid continuum generation from the windows. Laser-induced fluorescence was collected perpendicular to the laser propagation direction, collimated into a 20 cm monochromator (bandwidth 6 nm fwhm), and detected by a photomultiplier tube. The relative timing between the two pulses was varied with a high-precision, computer-controlled actuator located in the path of the pump laser. The pump arm also contained two polarizers and a half-wave plate to allow variation in the angle between the polarizations of the two lasers, and this angle was kept constant at 54.7° unless rotational anisotropy effects were under study. Studies of the anisotropy at high pressures will be reported later.

The home-built high-pressure cell was designed to withstand pressures of up to 4000 bar. The input window was 4.0 mm thick quartz, while the output and fluorescence-collection windows were 2.8 mm thick sapphire. Pressure inside the cell was monitored with a precision strain gauge pressure transducer, and the high-pressure cell showed no decrease in gas pressure during the course of an experiment. Fluorescence signal from the PMT was averaged in a boxcar integrator and recorded with a computerized setup as a function of actuator position. Data were analyzed with the help of a computer.

III. Results and Discussion

Here, all experiments have been performed using 60 fs pulses centered at 620 and 310 nm. In the accompanying paper,[4] we report the probe wavelength dependence. In most experiments, the ion-pair state fluorescence from the D′ → A′ state has been detected. The detection wavelength varied from transient to transient depending on the solvent-induced red shift of the transition, as discussed before. In some experiments in helium or neon, a detection wavelength of 270 nm has been used. In all experiments, the relative polarization between pump and probe lasers was set at 54.7°.

TABLE 1: Experimental Results for the Dissociation and Geminate Recombination of Iodine in Compressed Helium at 293 K as a Function of Solvent Pressure p and Density ρ[a]

p (bar)	ρ (mol/L)	τ_{pred} (ps)	τ_{fast} (ps)	a_{fast}/a_{pred}	a_{rec}
25	1.0	150.0	53	0.52	0
50	2.0	75.5	34	0.54	0
100	3.9	39.2	18	0.61	0
150	5.8	30.5	10	0.48	0
200	7.5	25.3	5.6	0.36	0
201	7.5	25.0	4.8	0.44	0
300	10.8	15.5	4	0.44	0
400	13.9	10.5	3.4	0.52	0
403	13.9	10.7	3.1	0.49	0
405	14.0	10.7	3.2	0.52	0
600	19.3	7.9	2.22	0.37	0
800	24.2	6.1	1.77	0.24	0
803	24.3	6.4	1.27	0.28	0
1200	32.1	4.2	1.3	0.23	0
1209	32.1	4.1	1.7	0.18	0.01
1394	35.7	3.7	0.8	0.11	0.01
1615	39.2	3.3		0.00	0.03
1960	44.4	2.8		0.00	0.05

[a] Experimental transients $s(t)$ are modeled by the sum of a biexponential decay and a single-exponential rise as described in the text: $s(t) = -a_{fast}\exp(-t/\tau_{fast}) + a_{pred}\exp(-t/\tau_{pred}) + a_{rec}(1 - \exp(-(t - t_0)/\tau_{rise}))$. The maximum of the B state transient at early times has been normalized to unity.

In general, the experimental transients can be characterized as follows. In all solvents and at all pressures, we observe an initial decay of the signal. The decay time, which is about 150 ps at 25 bar of helium (see Table 1), decreases monotonically with pressure and, at a given pressure, increases with solvent mass. The decay mainly reflects the population loss in the originally excited iodine B state due to solvent, collision-induced predissociation (see discussion below and accompanying papers). At very high pressures, this initial decay is followed by a rise in intensity. The amplitude of this rising transient relative to the initial B state signal intensity increases with pressure and, at a given pressure, with solvent mass. The rise time is also found to decrease with increasing pressure. The signal intensity at long times arises predominately from geminately recombined iodine molecules on the A/A′ states, and its rise time reflects the recombination dynamics and the subsequent vibrational relaxation within the A/A′ state.[4] Another main characteristic of the experimental transients is the coherence of the oscillatory wave packet. These different aspects of the dynamics of iodine in rare-gas solvents, i.e., coherent wave packet dynamics on the B state, B state predissociation, and geminate recombination, will be addressed separately in the next sections. First, however, we consider the effect of solvent polarity on iodine in different states.

III.1. Solvent Effect on the Solute Dipole. In this section, we consider the influence of solvent pressure on the fluorescence emission spectra from iodine *ion-pair* states. All fluorescence emission spectra were recorded after excitation of the iodine sample with temporally overlapping 620 nm pump and 310 nm probe pulses. This corresponds to a double-resonance excitation from the electronic ground state X to the B state and from the B to either the f or E ion-pair state.

The interpretation of the iodine fluorescence emission spectra is particularly simple in the case of argon solvent. It is known[70] that even at mild pressures of argon buffer gas ($p \geq 1$ bar), the iodine ion-pair state emission spectrum is dominated by fluorescence from the strong D′ → A′ transition (centered around 342 nm at low pressures, see Figure 4a). This emission is induced by a very efficient collision-induced electronic conver-

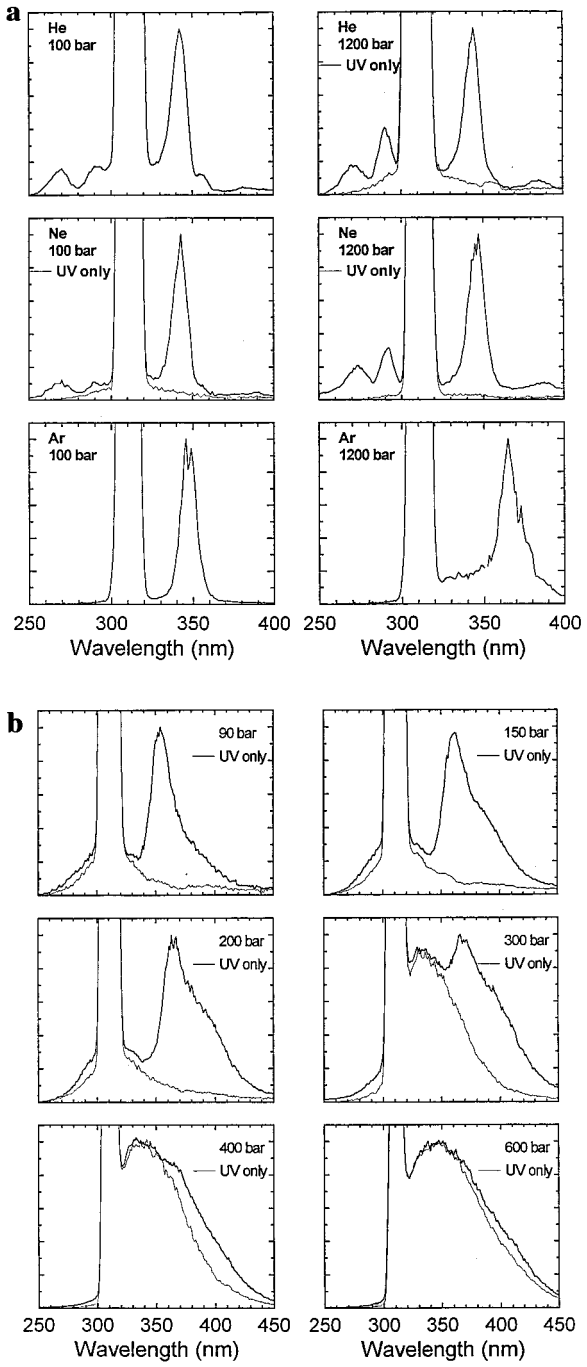

Figure 4. (a) Fluorescence emission spectra of iodine in compressed rare gases. Excitation was with temporally overlapping 620 nm pump and 310 nm probe pulses. In addition to the strong D′ → A′ emission around 342 nm, two additional bands around 270 and 290 nm are present in helium and neon (see text). In argon solvent, fluorescence emission originates entirely from vibrationally relaxed levels of the energetically lowest D′ ion-pair state. Note the strong solvent-induced red shift of the D′ → A′ transition in argon, indicating a strong solvation of the D′ state. The emission around 310 nm is due to scattered probe laser light. (b) Fluorescence emission spectra of iodine in krypton after two-photon excitation (620 + 310 nm). As in argon, only one emission band, the D′ → A′ transition, is observed. Note the solvent-induced red shift and the severe broadening of this transition at high pressures. At pressures above 200 bar, a broad band emission, due to one-photon excitation by the 310 nm probe laser, is detected. The intensity of this transition increases drastically with pressure, and at 600 bar the spectrum is entirely dominated by this band. The new emission is tentatively assigned to a charge-transfer transition of iodine−solvent complexes (see text).

sion from the originally excited f or E ion-pair state into the energetically lowest D′ ion-pair state, followed by a rapid vibrational relaxation within the D′ state. It is also known from resonance Raman experiments,[57] as well as from spectroscopic studies in large clusters and in rare-gas matrices,[71] that the potential energy curves of iodine valence states in solution are similar to their gas-phase potentials. In contrast, the ion-pair states are strongly affected by the solvent. This is due to the solvation of the molecular dipole of iodine in the ion-pair states, depending on the dielectric properties of the solvent. The solvation gives rise to a strong red shift of the D′ → A′ emission band from 342 nm at 0 bar to 357 nm at 400 bar and 368 nm at a pressure of 2000 bar. This corresponds to a solvation energy of about 2000 cm^{-1} at 2000 bar (Figure 4).

The pressure dependence of this red shift can be understood in terms of the classical cavity cell models of solvent shift.[72,73] The solvation models assume a nonpolarizable point dipole in the D′ state which is isolated in the center of a cavity in a uniform dielectric medium. The spectral shift in energy is then given as[74]

$$\Delta E = \frac{\epsilon - 1}{2\epsilon + 1}\frac{\Delta(\mu^2)}{a^3} \qquad (1)$$

where ϵ is the static dielectric constant of the solvent (for rare gases at high pressures see ref 75), $\Delta(\mu^2)$ is the difference in the squares of the ground- and excited-state dipole moments, and a is the diameter of the cavity, which is assumed to be pressure-independent. As shown in Figure 5, the theoretically suggested linear relationship between solvent-induced red shift ΔE of the D′ → A′ transition and $(\epsilon - 1)/(2\epsilon + 1)$ can be verified experimentally. The solvation of the D′ ion-pair state in high-pressure argon should be compared to the strong solvation of this state in large ultracold Ar_n clusters.[71] Here the intensity maximum of the D′ → A′ transition is shifted to ∼400 nm (corresponding to a solvation energy of 4240 cm^{-1}), similar to iodine in low-temperature argon matrices, where the shift is to 380 nm (or 2920 cm^{-1} of solvation shift).[76]

In helium and neon, the fluorescence emission spectrum at 100 bar is again dominated by the strong emission around 342 nm. In addition, emission bands are present at 270, 290, and around 385 nm (see Figure 4a). Similar bands have been observed in the emission spectrum obtained by optical double-resonance excitation of the $f0_g^+$ ion-pair state in the absence of buffer gases.[66] These bands were assigned[66] to the transitions $f0_g^+ \rightarrow B0_u^+(^3\Pi)$ (around 340 nm), $f0_g^+ \rightarrow B''1_u(^1\Pi)$ (around 290 nm), $f0_g^+ \rightarrow A1_u(^3\Pi)$ (around 280 nm), and $F0_u^+ \rightarrow X0_g^+(^1\Sigma)$[77] (250−272 nm;[78] the F state is thought to be populated through collisional energy transfer[66]). In high-pressure helium and neon, the $f0_g^+ \rightarrow B0_u^+(^3\Pi)$ band at 340 nm is likely to be overlapped by D′ → A′ emission, originating from B state molecules which are excited into the E ion-pair state and then collisionally quenched into low vibrational levels of the D′ state. Our spectroscopic results indicate that the electronic conversion between the f and D′ ion-pair states (which is very efficient in argon even at low pressures) is absent on the time scale of the ion-pair state fluorescence in helium and neon even at high pressures.

The solvation of the ion-pair states in helium and neon is far less pronounced than in the case of argon. The central wavelength of the 342 nm transition in helium shifts by only 3 nm (corresponding to a solvation energy of ∼200 cm^{-1}) to 345 nm if the helium pressure is increased from 0 to 2000 bar. Similarly, in neon a red shift of ∼450 cm^{-1}, from 342 to 347.5 nm, is observed. This indicates that, among the rare gases, helium and neon are unique; the potential energy curves of the iodine valence states as well as those of the ion-pair states are

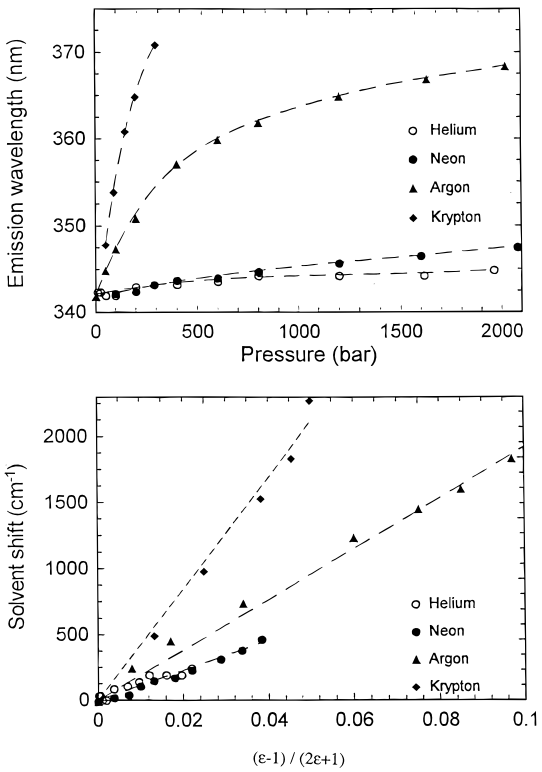

Figure 5. (top) Emission wavelength of the D′ → A′ transition in the compressed rare gases helium, neon, argon, and krypton. (bottom) Solvent-induced red shift of the D′ → A′ transition as a function of $(\epsilon - 1)/(2\epsilon + 1)$ in compressed rare gases. The solid lines are linear interpolations between the experimentally observed red shift and $(\epsilon - 1)/(2\epsilon + 1)$ as suggested by the classical cavity model (see eq 1). ϵ is the static dielectric constant of the solvent.

only weakly affected by the solvent. This feature makes these systems particularly attractive for investigation of the effect of solute−solvent collisions on the dynamics since many aspects of the dynamics can be modeled by assuming gas-phase isolated molecule potentials. The pressure dependence of the solvation energy in helium and neon follows the classical solvent shift model that is underlying eq 1, as shown in Figure 5.

In krypton (Figure 4b), a strong perturbation on the ion-pair states is noticed. As in argon, only one emission band, centered around 342 nm (at pressures of less than 5 bar), is observed, and this emission system is assigned to the D′ → A′ transition. The center wavelength of this transition shifts strongly with increasing pressure (to about 370 nm at 300 bar). Unlike in argon, an increase in pressure significantly broadens this transition. At intermediate pressures, the emission band shows a pronounced tail toward longer wavelengths which extends to the red of 430 nm at $p = 200$ bar (Figure 4b). At pressures of more than 200 bar, a new, broad band fluorescence is induced by the 310 nm probe laser, and the spectral range of this fluorescence extends from 310 nm to more than 450 nm in the red. The intensity of this transition increases drastically with pressure, such that, at $p = 600$ bar, almost the entire fluorescence spectrum is dominated by this new fluorescence band. This strong background fluorescence makes the detection of the overlapping D′ → A′ fluorescence very difficult and prohibited the extension of our experiments to higher krypton pressures. While the significant red-shift (to 423 nm) and the severe broadening of the transition have also been reported by Heaven et al. in cold krypton matrices, no broad band fluorescence was monitored in their experiments for one-photon excitation at 308 nm. Absorption at 308 nm cannot be caused by bound electronic states of iodine. It is known, however that iodine molecules in complexing solvents like CS_2, benzene, toluene, or dioxane give rise to a very intense broad band absorption around 300 nm,[79] which is assigned to a charge-transfer transition of iodine−solvent complexes.[80] (For a recent study of the fs dynamics of such complexes see refs 81 and 82.) It is likely that the presence of such iodine−solvent complexes in krypton at high pressures is the origin of the strong broad band emission induced by absorption of 310 nm photons.

III.2. Coherent Wave Packet Dynamics. In an isolated iodine molecule, the fs excitation process creates a coherent vibrational wave packet on the excited B state.[16,17] The vibrational wave packet evolves according to the following superposition:

$$|\Psi_B(R)\rangle = \sum_i a_{XB}(v_i) \exp(-iE_i t/\hbar)|v_i\rangle \qquad (2)$$

where R is the internuclear iodine separation and $a_{XB}(v_i)$ are the amplitude coefficients of the wave function in the vibrational eigenstate i. The amplitude coefficients depend on the laser electric field G_{XB} and the transition dipole moment μ_{XB} between vibrational states in the X and B states. Coherences between the X and B surfaces are excluded here as they are not probed in the present experiments. The wave packet temporally evolves on the B state, and a second probe laser, centered at 310 nm, excites components of the wave function into vibrational levels of a higher lying ion-pair state $|v_i\rangle$. The population in the ion-pair state is detected by LIF. The final signal in the experimental transient is given by

$$I(t) \sim |\langle v_I|G_{BI}\mu_{BI}|\Psi_B\rangle|^2 \propto \sum_i |a_{XB}(v_i)|^2 |a_{BI}(v_i)|^2 + \sum_{i,j} a_{XB}(v_i)\, a_{BI}(v_i)\, a^*_{XB}(v_j)\, a^*_{BI}(v_j) \exp\left(-\frac{i(E_j - E_i)t}{\hbar}\right) + \text{c.c.} \qquad (3)$$

This can be reduced to[18] (see also accompanying paper)

$$I(t) \sim \sum_i A_i + \sum_{i \neq j} A_{ij} \cos[(E(v_j) - E(v_i))t/\hbar + \varphi_{ij}] \qquad (4)$$

which shows that the detected fluorescence signal is given as the sum of an "incoherent" part $\sum_i A_i$ and a "coherent" part which contains the oscillatory terms due to vibrational coherences on the B state. Coherences due to the ground state are eliminated since phase incoherent pulses and time-independent detection are used.

The coherences on the B state have been monitored experimentally over tens of picoseconds (see Figure 6). The magic angle transient and the Fourier transform of its oscillatory modulation (Figure 7) show that the fluorescence signal contains frequency components which correspond to energy differences $E(v_{i+1}) - E(v_i)$ between adjacent vibrational eigenstates of the B state. Higher frequency modes, corresponding to coherences between nonadjacent vibrational levels, can also be observed.[18] The magic angle transient shows directly the average vibrational frequency of the B state wave packet, and the interference pattern in the signal modulation originates from the distribution of different vibrational eigenstates that is excited by the pump laser pulse. The power spectrum amplitude A_{ij} of each component reflects the population of the states i and j and depends on the frequency spectrum of the light pulses and the electronic surfaces which are involved in the light−matter interaction. For a detailed analysis of experiments at different excitation energies and the extraction of the B state potential, a more general picture is required which also includes the

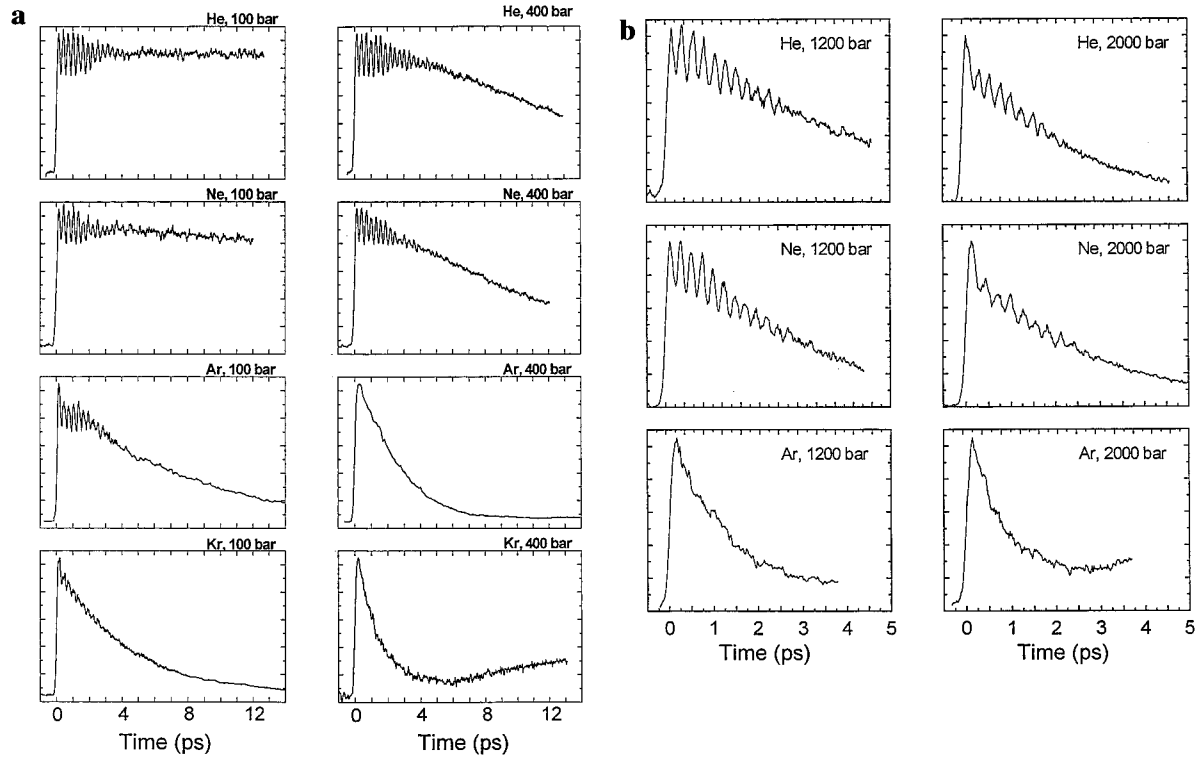

Figure 6. Vibrational dephasing and solvent-induced predissociation. (a) Femtosecond transients (up to 13 ps) for iodine in supercritical rare gases (helium, neon, argon, and krypton) at a temperature of 293 K and a pressure of 100 and 400 bar. The oscillatory modulation on the transients reflects the coherent vibrational motion within the B state, while the underlying decay is due to the collision-induced B state predissociation. Laser-induced fluorescence detection at the "magic angle" (54.7°) between pump (620 nm) and probe (310 nm) pulses was used. Fluorescence detection wavelength: helium and neon, 270 nm; argon, 348 nm at 100 bar and 360 nm at 400 bar; krypton, 354 nm at 100 bar and 390 nm at 400 bar. (b) Femtosecond transients (up to 5 ps) for iodine in supercritical rare gases (helium, neon, argon, and krypton) at a temperature of 293 K and at a pressure of 1200 and 2000 bar. In helium and neon, an oscillatory modulation of the transients is observed for more than 2 ps, indicating the long persistence of the coherent motion within the B state. The strong fluorescence intensity during the first oscillation on the 2000 bar transients in helium and neon is due to the probing of directly dissociating iodine molecules excited onto the $A1_u(^3\Pi)$ (34%) or $B''1_u(^1\Pi)$ states (and VR). Laser-induced fluorescence was detected at the "magic angle" (54.7°) between pump (620 nm) and probe (310 nm) pulses. Fluorescence detection wavelength: helium, 270 nm at 1200 bar and 342 nm at 1960 bar; neon, 270 nm at 1200 bar and 348 nm at 2080 bar; argon, 367 nm at 1200 bar and 375 nm at 2000 bar.

rotational motion of the iodine molecules. A complete treatment in terms of the density matrix formalism has been given by Gruebele and Zewail, and the reader is referred to ref 18.

In the absence of the iodine−solvent interactions, the wave packet can freely propagate on the B state which decays within microseconds. The phase coherence of the generated wave packet is maintained, and the decay of the oscillatory modulation of the magic angle transient on a time scale of approximately 40 ps results only from the difference in energies between the various vibrational−rotational states that are populated on the B state.

In the presence of iodine−solvent interactions in high-pressure rare gases, however, iodine−rare gas collisions will induce a dephasing of the coherences. In simple cases the coherence between two levels i and j may be assumed to decay exponentially, and a total dephasing rate $1/T_{2,ij}$ for this decay can be introduced. Moreover, iodine−solvent collisions will also cause a decay of the excited B state population via collision-induced predissociation onto a repulsive state. This predissociation causes a decay of the incoherent signal contribution. If exponential predissociation rates $1/T_{\mathrm{pred},i}$ are assumed, the total fluorescence signal in the presence of high-pressure rare gases may be written as

$$I(t) \propto \sum_i A_i \exp\left(-\frac{t}{T_{\mathrm{pred},i}}\right) + \sum_{i\neq j} A_{ij} \exp\left(-\frac{t}{T_{2,ij}}\right) \cos((E(v_j) - E(v_i))/\hbar + \varphi_{ij}) \quad (5)$$

From the fs time-resolved experiments we can thus obtain detailed information on the iodine dynamics: the decay of the incoherent signal contribution $I_{\mathrm{inc}}(t) = \sum_i A_i \exp(-t/T_{\mathrm{pred},i})$, which gives the predissociation dynamics, and the coherent contribution $I_{\mathrm{coh}}(t)$, i.e., the oscillatory signal modulation, which reflects the coherent vibrational wave packet motion under the influence of iodine−solvent interactions.

An overview of the experimental transients in helium, neon, argon, and krypton at selected pressures of 100, 400, 1200, and 2000 bar is shown in Figures 6a,b. The decay of the incoherent signal due to predissociation is clear in all transients and will be discussed in detail in section III.3. In general, the predissociation rate increases with solvent density and polarizability. In the rare gases helium and neon, an oscillatory modulation is present on all transients, even at the highest pressures of this study. At pressures of 100 bar, the oscillatory modulation extends over more than 12 vibrational periods or 4 ps. Within the first 4 ps, the modulation on the transients resembles that of the 0 bar transient. At longer delay times, the 0 bar transient displays a strong recurrence of the signal modulation (centered around $\Delta t = 9$ ps). This recurrence modulation is almost entirely damped in the 100 bar transients. Only the 100 bar transient in helium displays slight coherences at delay times of more than 6 ps (clearly revealed through Fourier transformation of the experimental transient). At higher pressures (see the 400 bar transient in helium and neon, Figure 6a), the phase coherence in the B state wave packet is lost after 5 ps. Indications for a recurrence modulation at 9 ps are not observed. Interestingly,

as the pressure is further increased in helium and neon (Figure 6b), the coherent motion persists for at least 3 ps at a pressure of 1200 bar and at least 2.5 ps or eight vibrational periods at about 2000 bar, the highest pressure in our study here.

Surprisingly, the loss of the coherent vibrational motion is only weakly affected as the pressure is increased by a factor of 20 from 100 to 2000 bar in helium and neon. In argon, experimental results were first published for pressures up to 100 bar[20] and later at pressures of up to 800 bar. At a pressure of 10 bar, coherence was observed to persist for at least 15 ps; as the pressure increases to 100 bar, the coherence dephases more rapidly and is lost after 5 ps. At pressures as high as 800 bar, vibrational coherence persists for more than 1.5 ps (five vibrational periods). Unlike in the lighter rare gases helium and neon, the modulation depth of the oscillatory transient signal is found to decrease with pressure, which might partly be due to dispersive temporal broadening of the laser pulses at higher argon pressures.

To obtain quantitative information on the vibrational dynamics in the presence of high-pressure rare gases, we first attempted to extract the frequency components of the oscillatory modulation of the signals at different pressures. We used two different approaches. First, we evaluated the Fourier transform spectra of the transients after subtraction of the overall population decay. The power spectrum of the 0 bar transient indicates the distribution of vibrational levels which are excited in the B state and reveals the energy differences between adjacent vibrational levels $E(v_{i+1}) - E(v_i)$. The amplitude of the component with frequency $\omega_{i+1,i} = E(v_{i+1}) - E(v_i)$ in the Fourier spectra is correlated with the population in the vibrational levels $i + 1$ and i. The maximum in the Fourier spectrum at 0 bar corresponds to the frequency $\omega_{8,7} = 113$ cm^{-1}, and the entire width of the Fourier spectrum reflects the number of vibrational eigenstates which are populated by the pump laser pulse. The width of each individual line in the spectrum is limited by the finite time delay (20 ps) up to which the experimental transient was recorded.

At a helium pressure of 100 bar, the Fourier spectrum broadens significantly, and this is due to the solvent-induced dephasing. Nevertheless, several distinct frequency components are resolved, and we note that the intensity of components with a frequency of more than 114 cm^{-1} increases significantly compared to the 0 bar transient; the entire spectrum thus shifts to higher frequencies. The fact that the spectrum displays distinct frequency components indicates the persistence of vibrational coherence for more than 5 ps and that the weak recurrences observed in the real time transient for delay times of about 8 ps are not due to noise. The broadening of the spectrum is even more pronounced as the pressure is increased to 400 bar. The spectrum is almost entirely smeared out; only a weak shoulder at low frequencies can be resolved. The entire spectrum shifts to higher frequencies; the amplitude maximum is now centered at 115 cm^{-1}. At the highest pressure of 1960 bar, the spectrum is structureless, significantly broader than at the lower pressures and strongly blue-shifted to a center of ~118 cm^{-1}. The results are summarized in Figures 7 and 8. The mean vibrational frequency of the oscillatory signal modulation (as determined from the intensity maximum in the power spectra) increases with pressure from 113 cm^{-1} at 0 bar to ~118 cm^{-1} at 2000 bar.

To confirm this finding, a second, different method was adopted to determine the mean vibrational period. The transient oscillatory modulation was fit to an exponentially damped phase-shifted cosine function $a \exp(-t/\tau_d) \cos(\omega_m t + \varphi)$. Fits to the experimental transients are displayed in Figure 7. The overall quality of the fits is satisfactory, although some features (e.g., weak recurrences of the modulation on the 100 bar transients in helium after about 8 ps) are not reproduced. The mean oscillatory frequencies that are obtained by this method are,

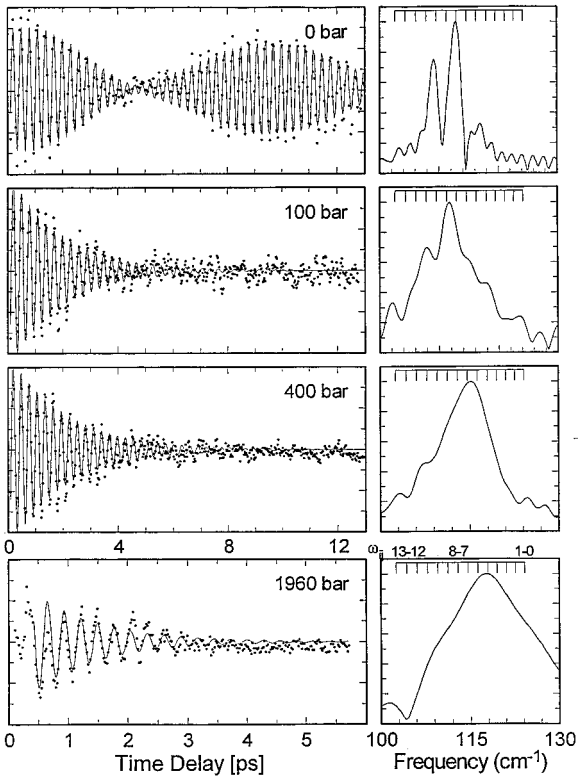

Figure 7. Vibrational dephasing in helium. Left side: oscillatory modulation on the femtosecond transients after subtraction of the underlying decay due to solvent-induced predissociation. Dots: experimental data points. Solid lines: fits of the transients to an exponentially damped, phase-shifted cosine function $a \exp(-t/\tau_d) \cos(\omega_m t + \varphi)$. Note the rapid dephasing at a helium pressure of 100 bar compared to 0 bar, but the persistence at higher pressures. "Magic" angle polarization between pump (620 nm) and probe (310 nm) wavelengths was used. Detection wavelength: 270 nm at 0 and 1960 bar and 342 nm at 100 and 400 bar. Note the change in time scale for the last panel. Right side: fast Fourier transform (power spectrum) of the oscillatory modulation. At 0 bar, the Fourier spectrum reveals the energy differences between adjacent vibrational B state levels $\omega_{ij} = \omega(i) - \omega(j)$. The distribution of vibrational levels, which is excited by the pump laser, reaches $v' = 6$ to $v' = 11$ and is centered around $v' = 8$. As the helium pressure increases, the Fourier spectrum broadens and shifts to higher frequencies.

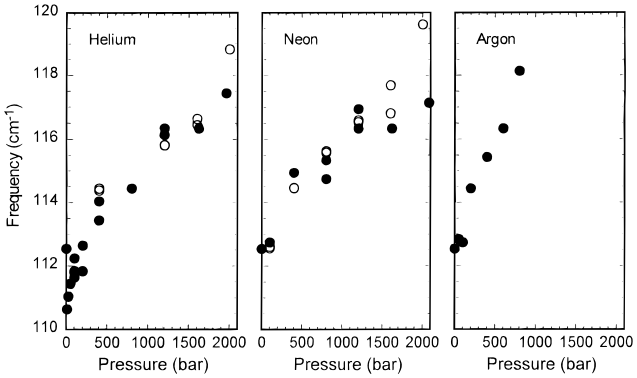

Figure 8. Pressure and solvent effect on the mean vibrational frequency of the B state wave packet motion in the rare gases helium, neon, and argon. Filled circles indicate mean frequencies of the Fourier spectra of the oscillatory transient modulation. Open circles are frequencies ω_m obtained from fits of the oscillatory modulation of the experimental transients to an exponentially damped phase-shifted cosine function $a \exp(-t/\tau_d) \cos(\omega_m t + \varphi)$.

within the experimental error, similar to those obtained from the Fourier spectra. The increase in frequency with pressure is reproduced. An analysis of the transients in neon and argon confirms these observations; in each solvent the mean oscillatory frequency increases with pressure, from 112.5 cm^{-1} at 0 bar to about 118 cm^{-1} in neon at 2080 bar and to 118 cm^{-1} in argon at 800 bar, respectively. In fact, the shift of the mean oscillatory frequency appears to increase linearly with pressure, roughly with a slope of a few wavenumbers per kilobar; a more quantitative description for the density dependence will be given in the accompanying paper. These are rather substantial shifts, considering that experimentally observed solvent-induced frequency shifts on ground-state iodine in nonpolar liquids are more on the order of 1−2 cm^{-1}.[83]

We now consider these experimental findings to address the nature of solute−solvent interactions. A theoretical hard-fluid model for solvent-induced frequency shifts in solutions was presented by Ben-Amotz and Herschbach.[84] The model considers a diatomic oscillator in a benign solvent and assumes that the net frequency shift $\Delta\nu = \Delta\nu_R + \Delta\nu_A$ is the resultant of a positive contribution from repulsion and a negative one from attraction. Vibrational frequency shifts calculated with their model have been checked against experimental results for a variety of solutes and solvents, especially for ground-state iodine and pyridine.

If the vibrational potential U_0 of the isolated (gas-phase) solute oscillator is written as

$$U_0(r_{12}) = {}^1/_2 f(r_{12} - r_e)^2 + {}^1/_2 g(r_{12} - r_e)^3 \qquad (6)$$

and if its interaction with the solvent is described by the potential of mean force,

$$V_{\text{mean force}}(r_{12}) = F(r_{12} - r_e) + G(r_{12} - r_e)^2 \qquad (7)$$

an expression for the frequency shift is obtained:[83]

$$\Delta\nu(n\leftarrow 0)/\nu_0(n\leftarrow 0) = n(F/f)[-(3/2)(g/f) + (G/F)] \qquad (8)$$

This gives the frequency shift $\Delta\nu$ for the $v = 0 \rightarrow v = n$ transition, normalized to ν_0, the isolated molecule (gas-phase) frequency. The frequency shift is predicted to be proportional to the vibrational quantum number n, and thus $\Delta\nu(n\leftarrow n-1) \approx \Delta\nu(1\leftarrow 0)$.

The result of the hard-fluid model of Herschbach and Ben-Amotz is attractive in that it gives an analytical expression for a cavity distribution function which pertains to a pair of hard-sphere solute atoms dissolved in a hard-sphere solvent. It thus provides a measure of the packing forces experienced by the (iodine) diatomic solute as a function of interatomic separation. Knowledge of this distribution function now allows one to directly compute the repulsive contribution to the potential of mean force and therefore to the solvent-induced frequency shift using eqs 6−8. In the accompanying paper, we invoke MD simulations to compare with experiments.

To calculate the attractive contribution to the frequency shift, the model of Herschbach and Ben-Amotz employs a van der Waals mean field approximation.[85,86] This approximation implies that the attractive shift is linearly proportional to the solvent density ρ

$$\Delta\nu_A(n\leftarrow 0) = nC_A\rho \qquad (9)$$

According to a procedure described by Schweizer and Chandler,[85] for (ground-state) I_2 in nonpolar solvents, the constant C_A is estimated to be $C_A \approx 0.061\alpha$, where α denotes the solvent polarizability. Assuming that this approximation is also roughly valid for iodine in the B state, eq 8 can be used to analytically calculate solvent-induced vibrational frequency shifts in rare gases as a function of pressure. The results of these calculations are shown in Figure 9. Two conclusions can be drawn from these model calculations. First, the polarizability of the rare gases helium and neon is so small that in these rare gases attractive solute−solvent interactions are of minor importance. The solvent-induced frequency shift is dominated by the repulsive interaction, and the iodine vibrational frequencies are blue-shifted toward higher frequencies. In argon, however, the polarizability is larger, so that attractive forces become dominant at lower solvent densities, and a weak red shift is expected at low pressures. A similar change from solvent-induced red to blue shift with increasing solvent densities has been observed experimentally for ground-state iodine in liquid alkane solvents.[84] The magnitude of the net solvent-induced vibrational frequency shift predicted by the model is less than 2 cm^{-1} for all solvents and at all pressures used in our experiments.

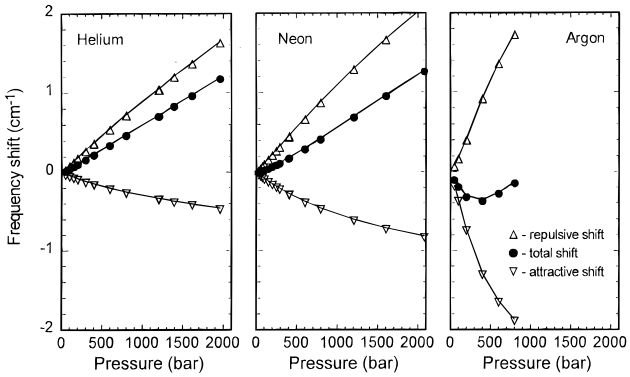

Figure 9. Theoretical estimate of the solvent-induced vibrational frequency shift for B state iodine in helium, neon, and argon according to the hard-fluid model. The total frequency shift $\Delta\nu = \Delta\nu_R + \Delta\nu_A$ is the resultant of a positive contribution from repulsive and a negative one from attractive solute−solvent interactions. We note that the theoretically predicted shift is significantly smaller than the experimentally observed shift on the mean iodine vibrational frequency (see Figure 8); see text.

In helium and neon, the theoretically predicted frequency shift is approximately proportional to pressure, and the proportionality constant is 0.6 cm^{-1}/kbar. In argon, it is close to zero for pressures below 1 kbar. These solvent-induced frequency shifts are substantially smaller than the experimentally observed shifts, so that we conclude that the solvent-induced change of the B state potential alone cannot explain our experimental findings. The following mechanism emerges and is supported by MD calculations (see accompanying paper). Due to collisions with solvent atoms, vibrational relaxation may take place on the time scale of vibrational dephasing. If the wave packet coherence is at least partially preserved during the inelastic collisions that lead to vibrational energy transfer between iodine and the surrounding solvent atoms, the mean vibrational energy of the iodine wave packet decreases on the time scale of the vibrational dephasing. The wave packet then shifts toward lower vibrational quantum numbers with time, and the mean frequency in the Fourier spectrum shifts toward higher energies, as is observed experimentally. Such conclusions are consistent with our recent MD simulations for these systems. This coherent energy relaxation has been found in liquid-state studies and discussed in relation to Redfield's equations.[87] The findings are relevant to experiments on dissociation and recombination of iodine in solid rare-gas matrices[60] and to studies of coherence in the photodissociation of I_3^-.[88] There is another relevance. The iodine−solvent interaction may shift the ion-pair states to

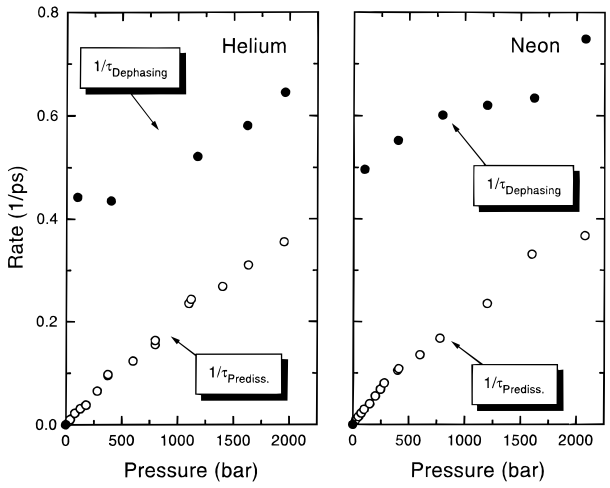

Figure 10. Vibrational dephasing and solvent-induced predissociation at high pressures for B state iodine in helium and neon. The filled circles give dephasing rate obtained by fitting the experimental data to a single exponentially damped cosine function. The open circles are for the predissociation rates. In the accompanying paper, we provide a wide range of measurements and their density dependencies.

lower energies, as discussed above. With increasing pressure the amplitude of the higher frequency components may increase, and this may also contribute to the observed shifts. Further experiments could follow the time evolution of, e.g., iodine molecules that are initially excited to higher vibrational B state levels. Such experiments would allow us to tune the vibrational energy of the initial wave packet and to follow the coherent vibrational energy relaxation.

Next, we focus on the *dephasing* of the coherent vibrational motion. In the most simple approach, the experimental transients at higher pressures can be fitted to a single damped phase-shifted cosine function $a \exp(-t/\tau_d) \cos(\omega_m t + \varphi)$, as displayed in Figure 7 and described above. Dephasing rates $1/\tau_d$ obtained by using this approach are given in Figure 10. The B state consists of a superposition of several different vibrational levels, and the transients are, therefore, a superposition of more than one damped cosine function. The beating between the frequencies of these modes leads to an apparent dephasing and rephasing of the oscillatory modulation even in the absence of solvent collisions, as seen in the 0 bar transient. As shown in the accompanying paper, even if all the frequencies are included, at about and above 100 bar, the fits indicate the predominance of one oscillation frequency whose relative value increases with density. Care should be taken in handling the transition to this regime. For example, by fitting the 0 bar transient to eq 5 and determining all frequencies and phases of the coherent signal, and then using these parameters in the analysis of all transients at higher pressures, we were able to reproduce the envelope of the coherent signal contribution

$$I(t) \propto \sum_i A_{i,i+1} \exp\left(-\frac{t}{T_2}\right) \cos[(E(v_{i+1}) - E(v_i))/\hbar + \varphi_{i,i+1}]$$

but with slower dephasing rates. (This is because of the coherence interference giving rise to an apparent dephasing.) However, this cannot be the case, as we know that the frequencies of the wave packet change with pressure and one frequency component dominates at higher pressure.

Dephasing rates $1/T_2$ are displayed in Figure 10 for the rare gases helium and neon. The results are plotted together with predissociation rates $1/T_{pred}$ as a function of pressure. While the predissociation rate increases nearly linearly with pressure from 0 ps^{-1} at 0 bar to about 0.4 ps^{-1} at 2000 bar in helium and neon, the dephasing rate displays a noncontinuous behavior. In the limit of low-pressure gases, $p \rightarrow 0$, dephasing rate $1/T_2$ and predissociation rate $1/T_{pred}$ approach zero. At a pressure of 100 bar, however, we find, using the single cosine approach, a dephasing rate of approximately 0.4 ps^{-1}, which is about 16 times faster than the predissociation rate in helium and neon at this pressure. Unlike the predissociation rate, the dephasing rate increases only slightly with pressure and approaches 0.7 ps^{-1} at the highest pressure of 2000 bar in helium and neon. (The complete range of values is given in the accompanying paper.)

In order to understand the pressure dependence of the rates, we need to address the physical origins of the dephasing between adjacent vibrational modes. In simple cases, the total dephasing rate may be written as the sum of the rates of the various processes[89−92] which cause the dephasing or phase relaxation of the wave packet. In general, four different physical phase relaxation mechanisms can be identified, *i.e.*, solvent-induced predissociation with a rate $1/T_{pred}$, vibrational relaxation, $1/T_{V-V}$, within the B state and vibration−rotation coupling, $1/T_{V-R}$ via inelastic collisions, and "pure" phase relaxation, $1/T_2'$ via elastic collisions. Assuming that for all these processes the relaxation rates of the coherence between adjacent vibrational eigenstates are independent of the vibrational quantum number, the total dephasing rate can be written as

$$\frac{1}{T_2} = \frac{1}{T_{pred}} + \frac{1}{T_{V-V}} + \frac{1}{T_{V-R}} + \frac{1}{T_2'} = \frac{1}{T_1} + \frac{1}{T_2'} \qquad (10)$$

The assumption of constant relaxation rates for the different vibrational B state levels is certainly not strictly correct but seems adequate since only average dephasing rates $1/T_2$ can be extracted from the time-resolved experiments and the disparity in the quantum numbers is not large.

The predissociation rates $1/T_{pred}$ can be extracted from the overall decay of the B state population. They vary nearly linearly with pressure. In the limit of high pressures, the rates for $1/T_2$ are larger than those for collision-induced predissociation, indicating the contributions of VR and T_2' processes. V−R processes are negligible at the highest pressures as shown in the accompanying paper. If T_2' processes are negligible, then, from eq 10, $1/T_{V-V}$ can be obtained. The value for the dephasing time T_2 achieved in helium at 2000 bar is 1.3 ps, which is a factor of 5 longer that that reported for I_2 in liquid hexane (230 fs).[56]

At lower pressures, a different dephasing mechanism dominates. The dephasing rate is significantly faster than the predissociation rate, by about 16 times in helium at 100 bar. The mechanism can be identified by investigating the pressure dependence of the dephasing rates for the different processes. In the next section, we discuss the pressure dependence of the predissociation rates described on the basis of an isolated binary collision model; the predissociation rate is given as the product of a predissociation probability per collision p_{pred} and the frequency of iodine−solvent collisions z_{I_2-RG}

$$1/T_{pred} = p_{pred} z_{I_2-RG} \propto \rho_{RG} \qquad (11)$$

Similarly, the rate for vibrational relaxation can be written as the product of a probability for collisional deactivation per collision p_{V-V} and the collision frequency z_{I_2-RG}

$$1/T_{V-V} = p_{V-V} z_{I_2-RG} \propto \rho_{RG} \qquad (12)$$

As discussed above, the collision frequency in rare gases is

proportional to the density ρ_{RG} and, in helium, roughly proportional to pressure. Consequently, the vibrational relaxation rate $1/T_{V-V}$ shows the same pressure dependence as the predissociation rate $1/T_{pred}$. Since in the limit of high pressures the total dephasing rate is no more than a factor of 2 larger than the predissociation rate, we can conclude that $1/T_{V-V} \leq 1/T_{pred}$.

A similar argument holds for the "pure" phase relaxation caused by elastic iodine rare-gas collisions. The collisional interaction between the iodine oscillator and a rare-gas atom causes fluctuations in the iodine vibrational frequency. Since the collisions at different molecules are uncorrelated, the phase coherence among the ensemble of iodine oscillators is destroyed by the collisions. In the binary collision model of Fischer and Laubereau,[93] the phase relaxation rate $1/T_2'$ is proportional to the square of the phase shift $\Delta\varphi$ caused by one collision and the collision frequency:

$$1/T_2' = p\Delta\varphi^2 z_{I_2-RG} \propto \rho_{RG} \tag{13}$$

This model gives an analytic expression for the pure dephasing rate. It is interesting that at a pressure of 2000 bar, $1/T_2'$ is on the order of 20 ps in helium and 10 ps in neon, taking the typical parameters given in ref 93. Thus, T_2' is larger than T_{pred} and in this limit

$$\frac{1}{T_2} \cong \frac{1}{T_{pred}} + \frac{1}{T_{V-V}} + \frac{1}{T_{V-R}} \tag{14}$$

Contrary to the other dephasing mechanisms, in the high-pressure regime, the contribution of vibration−rotation interaction **decreases** with increasing pressure. This pressure dependence can be understood by examining the nature of vibration−rotation interaction. As is well-known, in each vibrational level the frequency of the iodine oscillator depends slightly on the rotational quantum number. Molecular collisions can thus indirectly cause vibration frequency fluctuations by inducing transitions between the rotational states with which the vibration is coupled. As long as the frequency of rotational transitions is much smaller than the frequency of iodine oscillator, simple collisional broadening should be an adequate description for this dephasing mechanism;[94] the dephasing rate $1/T_{V-R}$ and thus also the total dephasing rate $1/T_2$ should be proportional to the collision frequency or solvent density. In the limit of very rapid rotational relaxation the molecules undergo so many collision-induced transitions between rotational levels that, on the time scale of the vibrational period, all molecules tend to have the same mean rotational energy. It follows that as a result[95] of this "motional narrowing", in the limit of very high collision frequencies, rotationally inelastic processes no longer significantly contribute to the dephasing.

In the motional narrowing regime, dephasing rates $1T_{V-R}$ decrease with pressure,[96] which is consistent with our experimental results. Such a motional narrowing due to rapid rotational transitions has been experimentally observed for vibrational Raman line shapes of several molecules,[97,98] and the pressure dependence of the vibrational line shapes can be understood in terms of the Anderson−Kubo model.[99,100] A detailed theoretical analysis at different densities is given in the accompanying paper. We note that, in the limit of very high collision frequencies, the J-diffusion model by Brueck[101] becomes applicable, and the dephasing rate $1/T_{V-R}$ becomes *inversely* proportional to the collision frequency.

Finally, we note that for several experimental transients (Ar and Kr at 100 bar, He and Ne at 2000 bar) the fluorescence intensity of the first oscillation is significantly higher than at later times. At these early times the B state fluorescence signal is overlapped by fluorescence from molecules which are first excited by the pump laser above the dissociation limit of the A state and then by the probe into the D ion-pair state. Also, vibrational relaxation is part of the predissociation, as discussed later.

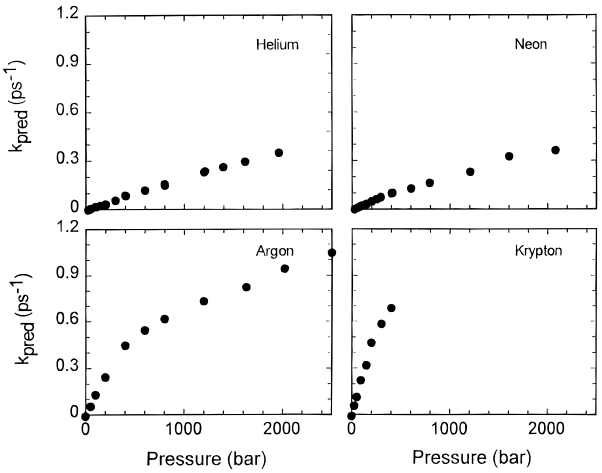

Figure 11. Collision-induced predissociation rates for B state iodine in compressed rare gases (helium, neon, argon, and krypton) at pressures between 0 and 2500 bar and at a temperature of 293 K. Excitation is at 620 nm.

III.3. Predissociation Dynamics: The Role of the Solvent. In the presence of iodine−solvent collisions, the population of iodine molecules in the B state is quenched into other electronic states through three competing processes (for a review see ref 102): radiative decay with a lifetime τ_0, nonradiative decay due to predissociation induced by iodine−iodine collisions (characterized by the self-quenching rate $1/\tau_s$), and predissociation induced via iodine−solvent collisions, characterized by a quenching rate $1/\tau_q$. For the experiments reported here, the iodine−solvent collision-induced quenching rate is orders of magnitude faster than $1/\tau_s$ and $1/\tau_0$, which are both on the same order, and predissociation dominates the B state decay process, so that $k_{pred} \cong 1/t_q$. The decay of the B state signal, which is underlying the modulation due to the coherent wave packet motion, therefore arises from collision-induced coupling onto a repulsive potential, most likely either the $a1_g(^3\Pi)$ or the $a'0_g^+(^3\Sigma^-)$ state (or the B″ state). Both states cross the B state at low energies; $a1_g$ crosses near the outer turning point $v' = 1$ and $a'0_g^+$ crosses near $v' = 5$ (see Figure 1). A recent resonance Raman study by Xu *et al.*[54] in CCl_4 presents experimental evidence for the involvement of these states in the predissociation process.

In krypton and argon, the observed transient decays are single exponential at all pressures above 200 bar, and from these decays, one obtains directly the predissociation rate. In krypton, the single-exponential decay time varies from 15 ps at 25 bar to 1.4 ps at 400 bar (see Table 4 and Figure 11), and the rate increases, proportional to the density. A similar behavior is observed in argon, the predissociation rate increases monotonically with pressure from $(16\ ps)^{-1}$ at 49 bar to $(0.9)^{-1}$ ps at 2500 bar (Table 3). At a given solvent pressure, the predissociation rate in argon is about 2 times slower than that in krypton. In argon, at pressures below 200 bar, a slight nonexponentiality of the decay signal at early times was noted. The transient signal may be fit to a biexponential decay, with a fast decay rate which is about 3 times faster than the predissociation rate. The amplitude of the fast component is significantly smaller (at least 4 times) than that of the predissociation component. Because of the oscillatory modulation on the fluorescence signals (see

TABLE 2: Experimental Results for the Dissociation and Geminate Recombination of Iodine in Compressed Neon at 293 K as a Function of Solvent Pressure p and Density ρ[a]

p (bar)	ρ (mol/L)	τ_{pred} (ps)	τ_{fast} (ps)	a_{fast}/a_{pred}	a_{rec}	τ_{rise}
28	1.1	115	50	0.598	0	
52	2.1	61	27	0.575	0	
77	3.0	43	18.5	0.535	0	
101	4.0	33.4	12.5	0.516	0	
150	5.7	23.8	7.2	0.448	0	
200	7.5	17.6	6.6	0.49	0	
250	9.1	14.1	5.8	0.49	0	
290	10.4	12.1	4.8	0.48	0	
403	13.7	9.3	3.3	0.42		
410	13.9	9.2	3.6	0.379	0	
602	18.8	7.4	2.2	0.236	0.09	69
794	23.0	5.9	1.2	0.301	0.15	55
1206	30.3	4.2	1.1	0.144	0.275	33
1603	35.7	3	0.75	0.242	0.424	33
2080	40.9	2.7	0.6	−0.15	0.671	27

[a] Experimental transients $s(t)$ are modeled by the sum of a bi-exponential decay and a single- exponential rise as described in the text: $s(t) = -a_{fast}\exp(-t/\tau_{fast}) + a_{pred}\exp(-(t - t_0)/\tau_{pred}) + a_{rec}(1 - \exp(-t/\tau_{rise}))$. The maximum of the B state transient at early times has been normalized to unity.

TABLE 3: Experimental Results for the Dissociation and Geminate Recombination of Iodine in Compressed Argon at 293 K as a Function of Solvent Pressure p and Density ρ[a]

p (bar)	ρ (mol/L)	τ_{pred} (ps)	a_{rec}	τ_{rise} (ps)
49	2.1	16	0.00	
100	4.3	7.3	0.00	
200	8.7	3.96	0.04	
400	15.5	2.2	0.27	60
600	19.6	1.81	0.47	45
800	22.4	1.6	0.70	35
1200	26.0	1.35	0.97	20
1630	28.8	1.2	1.25	14
2020	30.7	1.05	1.42	11
2500	32.5	0.95		9

[a] Experimental transients $s(t)$ are modeled by the sum of an exponential decay and a single-exponential rise as described in the text: $s(t) = \exp(-t/\tau_{pred}) + a_{rec}(1 - \exp(-(t - t_0)/\tau_{rise}))$. The maximum of the B state transient at early times has been normalized to unity.

Figure 7), an accurate determination of this fast component is difficult.

At a given density, the rates in argon are about 30% slower than in krypton. A plot of the predissociation rate k_{pred} versus argon density (Figure 12) gives a straight line relationship for pressures below 1000 bar (densities less than 24 mol/L). Accordingly, a plot of k_{pred} versus pressure gives the same nonlinear dependence which is observed between density and pressure (see Figures 2 and 11). At higher pressures, however, we notice that the experimental predissociation rates are slightly faster than expected from the linear relationship between k_{pred} and ρ for $p < 1000$ bar. The deviations are between 5% and 15%, and we note that these deviations increase monotonically with increasing pressure.

In order to check the linear relationship between predissociation rate and density and to investigate the effect of the solvent on k_{pred}, we studied the predissociation dynamics in helium and neon at pressures between 25 and 2080 bar (see Figures 14 and 15). A striking difference between the transients in helium and neon, compared to those in argon and krypton, was the pronounced biexponentiality of the B state fluorescence decays, which was observed over almost the entire pressure range. All transient signals $s(t)$ have to be analyzed in terms of a sum of two exponentials:

$$s(t) = -a_{fast}\exp(-k_{fast}t) + a_{pred}\exp(-k_{pred}t) \qquad (15)$$

TABLE 4: Experimental Results for the Dissociation and Geminate Recombination of Iodine in Compressed Krypton at 293 K as a Function of Solvent Pressure p and Density ρ[a]

p (bar)	ρ (mol/L)	τ_{pred} (ps)	a_{rec}	τ_{rise}
25	1.1	15		0.000
50	2.3	8.2		0.000
92	4.7	4.32		0.000
148	8.4	3.06	0.228	26
199	11.5	2.12	0.510	25
300	15.4	1.69	0.664	17
400	17.7	1.44	0.911	22

[a] Experimental transients $s(t)$ are modeled by the sum of an exponential decay and a single-exponential rise as described: $s(t) = \exp(-t/\tau_{pred}) + a_{rec}(1 - \exp(-(t - t_0)/\tau_{rise}))$. The maximum of the B state transient at early times has been normalized to unity.

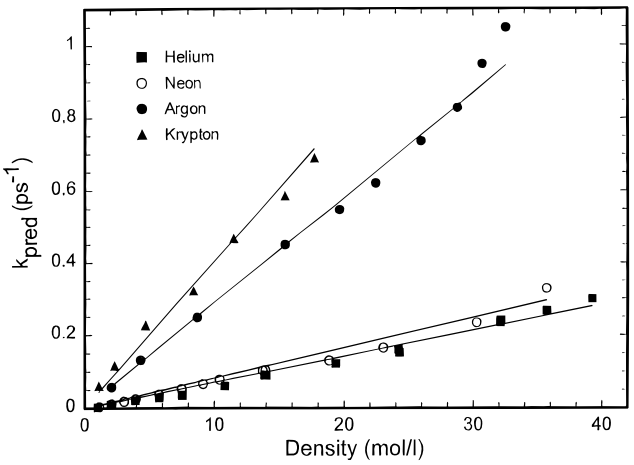

Figure 12. Collision-induced B state predissociation rates in rare gases (helium, neon, argon, and krypton) as a function of solvent density. The solid lines show linear interpolations between predissociation rate and density.

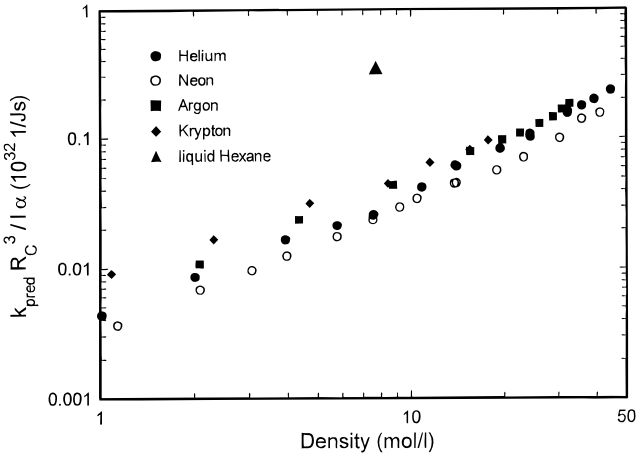

Figure 13. Reduced predissociation rates $k_{pred}R_c^3/I\alpha$ for iodine in helium, neon, argon, and krypton as a function of solvent density. Here, k_{pred} denotes the predissociation rate, R_c the distance of closest approach of the iodine−rare gas collision pair, I the ionization energy, and α the polarizability of the rare-gas solvent (see eq 22). According to the model, $k_{pred}R_c^3/I\alpha$ should be proportional to the solvent density, and the proportionality constant should be independent of the specific solvent. The model describes the entire set of experimental results in compressed rare gases reasonably well. The experimental value of the predissociation rate in liquid hexane, however, is 8 times faster than predicted by the model (see text).

As shown in Tables 1 and 2, the biexponentiality of the transient signal becomes more pronounced at low pressures; the ratio a_{fast}/a_{pred} is zero at the highest pressures and increases with decreasing pressure to more than 50% in helium and neon at pressures below 100 bar. At all pressures, k_{fast} is found to be

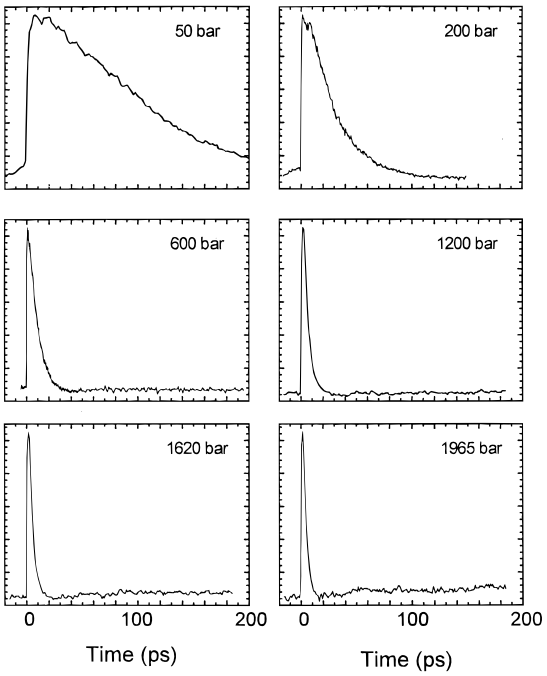

Figure 14. Predissociation and geminate recombination in helium. Experimentally observed transients (up to 200 ps) for iodine dissolved in helium at a temperature of 293 K and at pressures between 50 and 1965 bar. The fast fluorescence decay at early times shows the collision-induced B state predissociation. Note the strong variation in the B state lifetime. At the highest pressure, the fluorescence decay is followed by a weak increase in signal intensity, and this signal buildup at long times reflects the geminate recombination and subsequent vibrational relaxation on the A/A′ state. Fluorescence detection was at 342 nm.

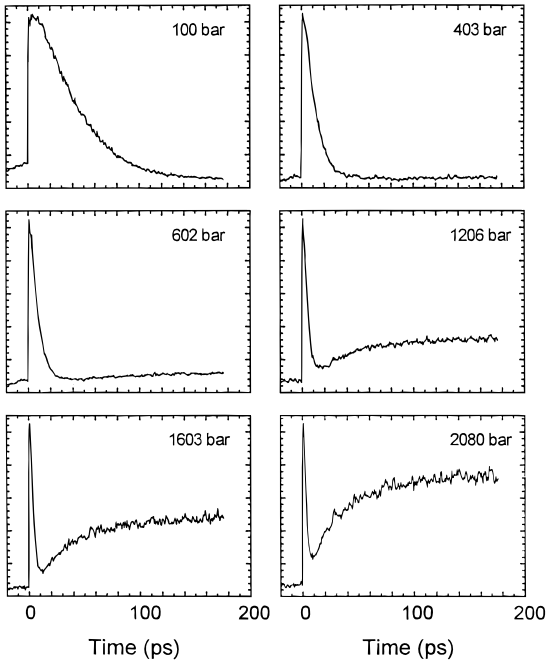

Figure 15. Predissociation and geminate recombination in neon. Experimentally observed transients (up to 200 ps) for iodine dissolved in neon at a temperature of 293 K and at pressures between 100 and 2080 bar. At a given pressure, B state decay times are similar to those in helium. Compared to iodine in helium, the fluorescence intensity at long times, and therefore the quantum yield for geminate recombination onto the A/A′ state is strongly enhanced. The recombination signal intensity persists (or increases slightly) for at least 1 ns. Fluorescence detection was at 343 nm−100 bar, 344 nm−403 bar, 344 nm−602 bar, 346 nm−1206 bar, 347 nm−1603 bar, and 348 nm−2077 bar.

approximately 3 times faster than k_{pred}. Several factors may contribute to the nonexponentiality of the fluorescence decays: (a) a variation in predissociation rate with vibrational quantum number (5−6 vibrational levels are initially populated by the relatively broad band pump pulse), (b) vibrational relaxation within the B state, and (c) a dependence of the absorption cross section for the probe laser on the B state vibrational level. A quantitative analysis of the exact shape of the transient requires more information about each one of these steps and will be attempted once experiments at varying pump wavelengths have been performed.

In helium and neon, the predissociation rates $k_{pred}(p)$ at a given pressure are found to be significantly slower than in argon or krypton. The difference in $k_{pred}(p)$ between helium and neon, however, was only minor (less than 10%). Again, at pressures between 0 and 1200 bar, the predissociation rate varies linearly with density (but not with pressure). As in the case of argon, the experimental predissociation rates at the pressures of 1600 and 2000 bar are slightly faster than expected from a linear extrapolation of the lower pressure rates versus density. Deviations are between 5 and 20% and increase at the highest pressures. An extension of these experiments to higher pressures enables us to examine the deviations from the proportionality between predissociation rates and density in further detail (see accompanying paper).

The fact that, up to very high pressures, the predissociation rate increases roughly linearly with density in all four rare gases indicates that the reaction rate k_{pred} can be written as the product of a binary collision frequency z_{I_2-RG} between iodine and the rare-gas solvent atoms and a probability for reaction per collision p_{pred}:[103]

$$k_{pred} = p_{pred} z_{I_2-RG} \tag{16}$$

For a simple hard-sphere, the collision frequency is

$$z_{I_2-RG} = \pi d_{I_2-RG}^2 \left(\frac{8kT}{\pi \mu_{I2-RG}}\right)^{1/2} N_A \rho = \sigma_{I_2-RG}\, \bar{v} N_A \rho \tag{17}$$

where the collision diameter d_{I_2-RG} is, for simplicity, taken as $d_{I_2-RG} = (d_{LJ}(I_2) + d_{LJ}(RG))/2$, with d_{LJ} being the Lennard-Jones diameter (m).[104] μ_{I_2-RG} is the reduced mass, σ_{I_2-RG} the cross section (m^2), and $\bar{v}$ the mean thermal velocity (m/s) of the collision pair. N_A is Avogadro's number and ρ the macroscopic solvent density (mol/L). This is valid in the low-density regime, as at higher densities (see accompanying paper), collision rates become nonlinear with density. An effective cross section for the predissociation reaction σ_{pred} can be defined as

$$\sigma_{pred} = p_{pred} \sigma_{I_2-RG} \tag{18}$$

and the predissociation rate is then given as

$$k_{pred} = \sigma_{pred} \bar{v} N_A \rho \tag{19}$$

(In the limit of low-pressure gases, $p \cong \rho RT$ and k_{pred} becomes proportional to pressure as suggested by the Stern−Volmer relationship.) The predissociation cross section σ_{pred} is obtained from a linear correlation between predissociation rate and solvent density. Such a correlation for pressures below 1200 bar resulted in the following values for σ_{pred}:

He, 0.98 Å^2; Ne, 2.20 Å^2; Ar, 11.1 Å^2; Kr, 21.4 Å^2

The same isolated binary collision approach has been extensively applied to low-pressure gas-phase reactions and here also to the electronic quenching of iodine. Quenching cross

sections at very low pressures of less than 10^{-3} bar (a pressure which is more than 6 orders of magnitude lower than the highest pressure reached in this study) have been obtained as a function of the excitation wavelength in a variety of gaseous atomic and molecular solvents.[105,106] At room temperature and at a foreign gas pressure of 4×10^{-5} bar, Capelle and Broida[106] measured quenching cross sections σ_{pred} of

He, 1.4 Å^2; Ne, 4.4 Å^2; Ar, 17.6 Å^2; Kr, 35.8 Å^2, for excitation at 623.4 nm

He, 1.1 Å^2; Ne, 2.6 Å^2; Ar, 16.0 Å^2; Kr, 30.5 Å^2, for excitation at 607.1 nm

These values are in reasonable agreement with those obtained in the present study given the range of density.

Thus, *although the solvent density is changed by more than 6 orders of magnitude, the physical mechanism which is causing the solvent collision-induced predissociation remains the same*, and isolated binary collisions seem to dominate even though the solvent "packing fraction" is similar to that in liquid solvents. This indicates that a short-range interaction causes the actual coupling between the bound and the repulsive state and that the actual "dissociation" of the molecule occurs only when iodine and the solvent atom are at very short internuclear distances. Up to rare-gas pressures of 1000 bar, multibody interactions are seemingly of less importance for the dissociation mechanism.

The good agreement between predissociation cross sections at very low and very high pressures indicates that theoretical models developed to predict low-pressure gas-phase predissociation rates may remain valid up to liquidlike densities. In the past, the model by Selwyn and Steinfeld[107] has been used in order to predict the solvent effect on the predissociation rates. In this approach, the collision between the excited iodine molecule and the solvent atom induces a time-dependent perturbation on the stationary iodine states and results in a transition between the excited B state and a repulsive state, which are degenerate but of different symmetry. During the collision, the symmetry of the B state is destroyed, and a coupling between both states can occur. In the case of uncharged, nonpolar species, this interaction arises from the dispersion forces induced between the iodine molecule and the quencher.[108] The model is based on a perturbation theory approach, which uses Fermi's "Golden Rule" to predict the predissociation rate.

The predissociation is attributed to a transition between the (ungerade) B state and a repulsive state (which therefore has to be of gerade symmetry). At a fixed distance R between iodine and the collision partner the predissociation rate in this perturbative treatment is proportional to the absolute square of the coupling matrix element between the zero-order bound-state wave function ψ_B and the wave function of the repulsive state(s) ψ_R under the interaction potential $V(R)$:

$$k_{pred}(R) = (2\pi/\hbar)\rho(E_R)\langle\psi_B|V(R)|\psi_R\rangle^2 \qquad (20)$$

where $\rho(E_R)$ equals the density of states on the repulsive potential at the excitation energy E_R. In order to obtain reaction probabilities or cross sections for a specific collision, the rate $k_{pred}(R)$ has to be integrated over time. This corresponds to a weighted averaging of reaction rates for different configurations during the collisional encounter. A parametric dependence of the reaction cross section on the solvent properties is obtained as

$$\sigma_{pred} \propto I\alpha\mu^{1/2}/R_c^3 \qquad (21)$$

The model indicates that three factors are of principal importance for the reaction probability, i.e., (a) the strength of electric-field-induced coupling between the bound and the repulsive state (proportional to the product of polarizability α and ionization energy I of the quencher molecule), (b) the duration of the collisional encounter (proportional to the mean thermal velocity and therefore to the square root of the reduced mass $\mu^{1/2}$), and (c) the distance of closest approach $R_c = {}^1/_2(d_{I_2} + d_{RG})$ of the collision pair. The following predissociation cross sections, normalized to σ(He) = 1.0 Å, were obtained:

He, 1.0 Å^2; Ne, 3.4 Å^2; Ar, 11.1 Å^2; Kr, 18.9 Å^2

in surprisingly good agreement with experimental results for the case of compressed rare gases. Furthermore, the model predicts that the experimentally observed change in the predissociation cross section with B state vibrational energy arises from the change in the Franck−Condon overlap between the B state and the repulsive state for different vibrational levels.

Equation 21 can now be used to obtain the following proportionality:

$$k_{pred}R_c^3/I\alpha = a\rho \qquad (22)$$

in which the proportionality constant a should be independent of the solvent. In fact, Figure 13 shows that eq 22 holds well for the rare-gas solvents under study, but not for example for liquid hexane. Here, the value for the B state predissociation rate of (230 fs)$^{-1}$ obtained by Scherer et al. was used. An extrapolation of eq 22 from the value of the predissociation rate in argon at 1600 bar, $k_{pred} = 1.05$ ps^{-1}, to liquid n-hexane predicts a predissociation rate of $k_{pred} = 0.5$ ps^{-1},[109] more than 8 times slower than the experimentally reported value k_{pred}(hexane) = 4.4 ps^{-1}. Of course, the model does not account for the effect of packing and radial distribution function, as discussed in the accompanying paper. Experiments in molecular solvents which bridge the gap between the gas and the liquid phase should be of great help for a detailed understanding of reaction dynamics in complex solutions.

III.4. Geminate Recombination: The Role of the Solvent. In this final section we will investigate the fate of the iodine atoms after predissociation, i.e., the process of recombination or caging by the solvent. In particular, we will emphasize studies of the geminate recombination of the dissociating pair of iodine atoms and its dependence on the properties of the solvent and the density. The excitation of iodine with the fs laser pulse leads to the formation of free ground-state iodine atoms, either through solvent-induced $B0^+_u(^3\Pi)$ state predissociation onto the repulsive $a1_g(^3\Pi)$ or $a'0^+_g(^3\Sigma^-)$ (or B″) state as discussed above (62% of the excited molecules) or through direct dissociation for those molecules which are excited onto the weakly bound $A1_u(^3\Pi)$ (34%) or the repulsive $B''1_u(^1\Pi)$ state (see Figure 1). The so-formed free iodine atoms will initially separate from each other under the influence of the repulsive interatomic potential and rapidly transfer their excess kinetic energy to the solvent.

At low pressures, the iodine atoms will then start a diffusive motion through the solvent. Diffusion coefficients at low pressures are relatively large, so that the atoms will soon reach large internuclear distances. For example, at an argon pressure of 100 bar, the diffusion coefficient for iodine atoms is about 10^{-7} m^2/s, so each atom travels ~0.3 nm/ps. Eventually, a free atom will collide with another iodine atom, most likely from a different parent molecule, and might undergo a solvent-mediated

atomic recombination

$$I + I + M \rightarrow I_2^* + M \quad (23)$$

where M denotes a solvent atom. Direct time-resolved measurements of second-order rate coefficients for this *nongeminate* recombination k_{rec}, defined as

$$d[I_2^*]/dt = k_{rec}[I]^2 \quad (24)$$

have been performed in a variety of gaseous and liquid solvents over a wide range of experimental conditions by the groups of Troe[29] and van den Bergh.[27,28] In compressed rare gases, nongeminate recombination occurs on a much longer time scale than the maximum time range of our experiment (1 ns). For example, at a pressure of 50 bar of argon, $k_{rec} = 4.6 \times 10^6$ m^3 mol^{-1} s^{-1}, and at a typical concentration of excited iodine molecules of[110] $c_0 = 4 \times 10^{-9}$ mol L^{-1}, we find a half-life for the nongeminate atomic recombination of $t_{1/2} = (4k_{rec}c_0)^{-1} =$ 15 ms.

As the rare-gas pressure is increased, a different recombination mechanism comes into play. A solvent shell or "cage" forms around the iodine molecules, and the rigidity of this solvent shell increases with density. The higher the pressure, the more likely it becomes that the atomic iodine fragments do not separate diffusely but become "caged" within this shell. These fragments from the same parent molecule can then undergo a nondiffusive, *geminate* recombination in which vibrationally excited iodine molecules I_2^* are formed on either the electronic ground state or on those bound electronic states which correlate with ground state iodine atoms, i.e., A or A′. In each of these bound states, the newly formed iodine molecules transfer their vibrational energy in a sequence of (deactivating and reactivating) collisions to the surrounding solvent atoms. Those iodine molecules which are formed in excited electronic states will eventually undergo an electronic transition to the ground state. The information that can be gained by our time-resolved experiments on this *geminate* atomic recombination process and the subsequent vibrational relaxation dynamics will be discussed below.

How can the newly formed iodine molecules I_2^* be observed in the time-resolved experiments? In the accompanying paper,[4] through the use of variable wavelength probe pulses, it is shown that the experiments are also sensitive to I_2^* molecules within the weakly bound A/A′ states. At a probe wavelength of 310 nm, molecules in low vibrational levels of these electronic states can be excited to higher lying ion-pair states and thus give rise to fluorescence at the same detection wavelength as molecules which are excited out of the B state. At sufficiently high pressures, it is therefore observed that the initially decaying fluorescence signal arising from predissociating B state molecules is followed by a recovery of the fluorescence intensity due to the probing of newly-born iodine molecules which are formed by geminate recombination. This fluorescence persists for at least 1 ns, and its temporal form can generally be described by a single-exponential rise $a_{rec}(1 - \exp(-(t - t_0)/\tau_{rise}))$, $t_0 > 0$. Both the signal amplitude a_{rec} and the rise time τ_{rise} are strongly solvent- and pressure-dependent, and this dependence is now discussed.

As the fluorescence arises from molecules in low vibrational A/A′ state levels, the rise time τ_{rise} reflects the dynamics of the geminate recombination act and the subsequent vibrational relaxation within these electronic states. It has been shown by Paige and Harris[53] that in liquid xenon the A/A′ state decay time due to electronic coupling to the ground state is longer than 5 ns. This A/A′ state decay is too slow to be resolved within the first nanosecond. The probe wavelength of 310 nm is *not* sensitive to probing the recombination dynamics onto the ground X state, and no information can be extracted on ground-state dynamics and "branching ratios" for recombination onto the different electronic manifolds.

In argon, through variation of the probe wavelength,[4] different vibrational levels of the A/A′ states can be probed. This allows one to separately study geminate recombination and vibrational relaxation dynamics. At high pressures, evidence was found for two geminate recombination channels. An "in-cage" primary recombination occurs within the first few picoseconds after dissociation. The primary recombination times decrease with increasing pressure from about 6 ps at 400 bar to less than 1 ps at 2500 bar, and primary recombination is significantly faster than the subsequent vibrational relaxation. Vibrational relaxation rates within the A/A′ states increase with pressure from 0.017 ps^{-1} at 400 bar to 0.13 ps^{-1} at 2500 bar. The second channel is a significantly slower, secondary diffusive geminate recombination of iodine atoms which takes place after the atoms leave the initial solvent cage and diffuse back to form molecular iodine. Secondary recombination constitutes a relatively smaller fraction (less than 30%) of the total geminate recombination. In the following, we focus on the pressure and solvent dependencies of the *probability* for this geminate recombination and the associated *dynamics*.

In helium (Figure 14), all transients (on a time scale of 0−200 ps) decay monotonically at pressures below 1200 bar. The rate of this initial predissociative decay increases with solvent density, as discussed above. At higher pressures, we notice a slight increase in the signal at long delay times. The recombination signal amplitude is small, and the probability for geminate recombination is therefore close to zero. In neon (Figure 15) the coherent and predissociation dynamics of the initially excited B state population are, at a given pressure, very similar to those in helium. At all pressures above 400 bar, the B state decay is followed by a recombination rise of the form $a_{rec}(1 - \exp(-(t - t_0)/\tau_{rise}))$, $t_0 > 0$. The recombination amplitude a_{rec} of this rise (relative to the maximum of the B state signal at early times, which has been normalized to unity) increases with pressure and reaches a value of 0.5 at the highest pressure of 2080 bar. The rise time, τ_{rise}, which reflects the time scale of the geminate recombination and the subsequent vibrational relaxation within the A/A′ state, decreases as the pressure increases: from 70 ps at 600 bar to about 27 ps at the highest pressure of 2080 bar.

In argon (Figure 16), recombination amplitudes that are larger than zero are observed at a pressure of only 200 bar. The recombination amplitude increases drastically with pressure (to 1.4 at 2020 bar),[111] and τ_{rise} decreases to less than 10 ps at the highest pressure. At pressures above 1200 bar, the recombination signals become distinctly nonexponential. We are able to fit the data to a biexponential rise with a fast rise time $\tau_{rise,fast}$ of, e.g., 11 ps at 1628 bar and a slow rise $\tau_{rise,slow}$ of about 100 ps and an amplitude of the slow relative to fast exponential rise of about 0.25. As discussed in detail in ref 4, this behavior indicates the presence of the two distinct geminate recombination channels: direct and diffusive. The fast rise reflects the direct "in-cage" recombination and the subsequent vibrational relaxation process, whereas the slow rise time is a measure of the much slower secondary diffusive recombination. At an argon pressure of 1600 bar, an in depth analysis of transients at a variety of probe wavelengths indicates a rate for "in-cage" recombination of 0.8 ps^{-1} compared to a rate of 0.005 ps^{-1} for the secondary diffusive recombination. Using this analysis, we find a vibrational relaxation rate within the A/A′ state of 0.08

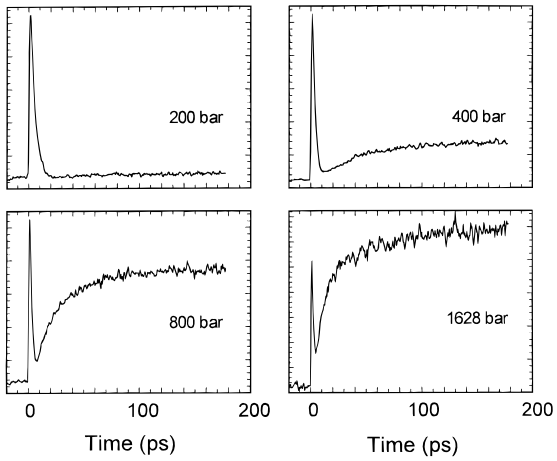

Figure 16. Predissociation and geminate recombination in argon. Experimentally observed transients (up to 200 ps) for iodine dissolved in argon at a temperature of 293 K and at pressures between 200 and 1965 bar. Compared to helium and neon, B state lifetimes times are significantly reduced. Note the pronounced biexponentiality on the recombination signal at a pressure of 1628 bar. Fluorescence detection was at 354 nm−200 bar, 360 nm−400 bar, 364 nm−800 bar, and 370 nm−1628 bar.

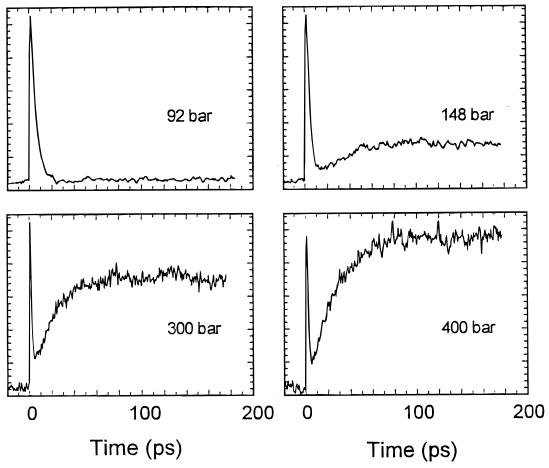

Figure 17. Predissociation and geminate recombination in krypton. Experimentally observed transients (up to 200 ps) for iodine dissolved in argon at a temperature of 293 K and at pressures between 92 and 400 bar. A significant intensity of fluorescence from newly formed iodine molecules is detected at a pressure of 148 bar. This intensity and thus the geminate recombination yield increase strongly with pressure. Fluorescence detection was at 354 nm−92 bar, 362 nm−148 bar, 385 nm−300 bar, and 390 nm−400 bar.

ps^{-1} at this pressure, which shows that the fast rise time at a probe wavelength of 310 nm is mainly determined by the vibrational relaxation rate. In krypton (Figure 17), the onset of geminate recombination is shifted to an even lower pressure value (less than 150 bar), and the recombination amplitude shows a stronger increase with pressure. At a krypton pressure of 400 bar, the recombination amplitude is close to unity. The experiments in krypton could so far not be extended to higher pressures for reasons that have been outlined above.

It is evident that the amplitude of the recombination signal reflects the probability for geminate recombination onto the A/A′ states. Under the assumption of pressure- and solvent-independent B and A/A′ state absorption cross sections at 310 nm, the observed recombination amplitudes are directly proportional to the quantum yield for geminate recombination onto the A/A′ state. This assumption appears realistic as the analysis of experimental and calculated absorption spectra shows that a probe wavelength of 310 nm is close to the absorption maximum in each state. Neglecting a possible solvent and pressure dependence of the branching ratio for caging onto the X and A/A′ state, the recombination amplitudes are proportional to the total quantum yield for geminate recombination, which, in krypton, has been obtained before from nanosecond experiments in the groups of Troe and van den Bergh. Using a value for the total quantum yield of $\phi_{rec}(Kr,400\ bar) = 0.4$, we can estimate the total quantum yield for geminate recombination as

$$\phi_{rec} = \frac{a_{rec}(p)}{a_{rec}(Kr,400\ bar)}\,\phi_{rec}(Kr,400\ bar) \qquad (25)$$

With this approximation, we find that in all solvents the geminate recombination yield is (close to) zero below a certain critical pressure. This critical pressure decreases with increasing solvent mass from about 1200 bar in helium, over 400 bar in neon and 200 bar in argon, to less than 150 bar in krypton. Above this critical pressure, the geminate recombination yield increases roughly proportional to the solvent pressure, and the proportionality constant between ϕ_{rec} and pressure increases strongly with increasing solvent mass. The quantum yield at the highest pressures of our study reaches 0.05 in helium (1960 bar), 0.29 in neon (2080 bar), 0.63 in argon (2500 bar), and 0.4 in krypton (400 bar). As the recombination quantum yield approaches its limiting value of unity, the linear relationship between quantum yield and pressure becomes invalid, as observed experimentally in the case of argon solvent at pressures above 1000 bar (Figure 16).

This change in the yield is related to the change in solvent structure with pressure, *i.e.*, the buildup of solvent cages and the increasing rigidity of the solvent cage with increasing pressure. Our experiments thus provide a link between time-resolved studies at low rare gas pressures and studies of the reaction dynamics in liquids, clusters, and rare-gas matrices. This is especially the case for studies in clusters and matrices which correspond to a (almost) perfectly rigid solvent cage and therefore to the limiting value of a geminate recombination quantum yield of unity.

In the past, several different theoretical approaches have been proposed to gain an understanding of the caging process. These approaches can be divided into three categories: (i) molecular dynamics simulations or multibody trajectory calculations:[112−116] (ii) classical stochastic trajectory simulations based on the molecular time-scale generalized Langevin equation (MTGLE) of motion for liquid state chemical reactions,[117−119] and (iii) diffusion-based models.[120−123] These latter models possess the advantage of providing analytical predictions for the pressure and solvent dependence of the key experimental observables, i.e., the geminate recombination yield and the caging time. Though being less rigorous than molecular dynamics or MTGLE simulations, these models are particularly attractive for a comparison of theoretical predictions to the experimental data. In the following, we will attempt a comparison of the experimental results to the diffusion-based model that has been proposed by Otto, Schroeder, and Troe (OST) for the atomic recombination of iodine and bromine in dense media.[29]

In this model (see Figure 18) the dissociation and recombination dynamics is split into two separate steps. The first is an initial separation of the two iodine atoms under the influence of their repulsive potential. During this separation step, the atomic fragments transfer their excess kinetic energy to the solvent. And, the second step is subsequent diffusive motion of the iodine atoms which occurs through the (continuous) solvent. In the first step, we assume that after predissociation

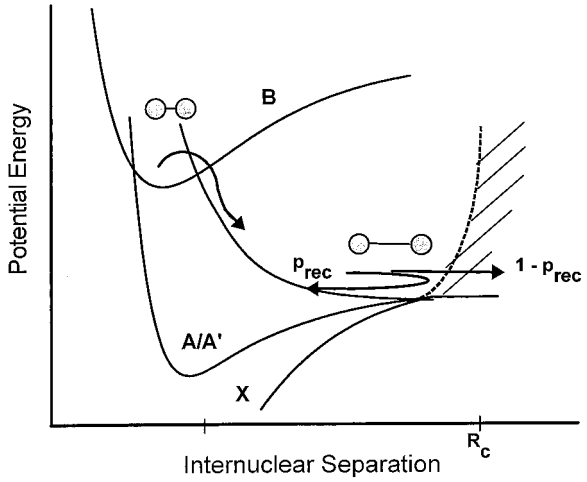

Figure 18. Model description of predissociation and geminate recombination of iodine in supercritical rare gases. After predissociation, the iodine atoms separate on the repulsive potential and transfer their excess energy to the solvent. There is a finite probability p_{rec} for breaking through the solvent barrier, located at encounter radius R_c, and this probability is strongly pressure and solvent dependent, as described in the text. The iodine atoms which remain within the solvent cage undergo direct or primary geminate recombination. Those which leave the solvent cage undergo a diffusive motion through the solvent and may recombine every time the atoms reach R_c. Such recombination acts after diffusive motion through the solvent are termed secondary.

the iodine atoms are placed on the repulsive $a0_g^+(^3\Sigma^-)$ or $a1_g$-$(^3\Pi)$ potential at an internuclear separation that corresponds to the crossing point of the respective electronic states at about $R_0 = 3.2$ Å. The atomic fragments then separate on the repulsive potential and transfer their excess energy to the solvent. In the OST model, it is assumed that the separating atoms experience a Stokes friction force by the (continuous) solvent and that, after energy equilibration, all atomic pairs reach a specific internuclear separation r_0. Typical initial separations r_0 are 43 Å in helium at 100 bar, 8 Å in krypton at 400 bar, and 6 Å in argon at 2000 bar; i.e., the higher the solvent viscosity, the more closely the fragments stay together.

At the highest pressures, r_0 lies within the range of the internuclear iodine−iodine potential. This is equivalent to saying that there is a large probability for finding the two iodine atoms inside the solvent cage. Starting from this internuclear separation r_0, all iodine atom pairs undergo a diffusive motion through the (continuous) solvent. In the OST model, the subsequent recombination process is treated in the following way. Every time the atomic fragments reach a certain critical encounter radius $R_c \leq r_0$, a finite probability p_{rec} for the formation of a new iodine molecule exists, and this recombination occurs through collisional deactivation by surrounding solvent atoms. The encounter radius R_c can be shown to be approximately given by

$$R_c \cong \{d_{LJ}(I) + d_{LJ}(M)\}/\sqrt{2} \tag{26}$$

where d_{LJ} denotes the Lennard-Jones diameter of I and the solvent atom M. As an example, in argon $d_{LJ}(I) = 4.320$ Å and $d_{LJ}(Ar) = 3.418$ Å; the encounter radius in neon is $R_c = 5.47$ Å.

The important parameter in the diffusion model is the recombination probability p_{rec}, which is given as

$$p_{rec} = \frac{k_{rec}^g}{k_{rec}^g + 4\pi R_c N_A D} \tag{27}$$

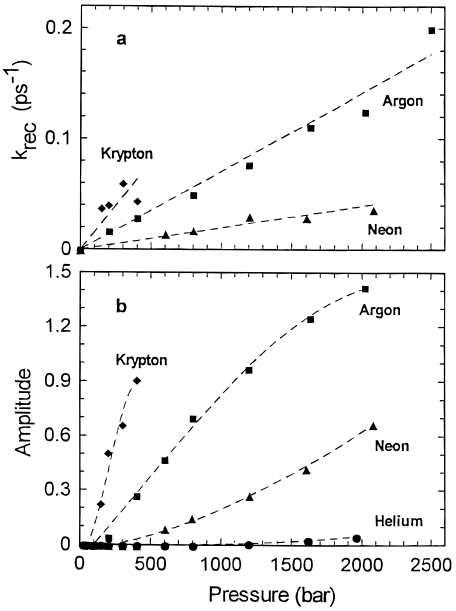

Figure 19. (top) Recombination rate $k_{rec} = 1/\tau_{rise}$ for iodine in neon, argon, and krypton as a function of pressure. These rates reflect the recombination dynamics of iodine atoms and the subsequent vibrational relaxation dynamics within the A/A′ states. (bottom) Amplitude of the LIF intensity at long times ($t = 170$ ps), relative to the initial B state signal (recombination amplitude a_{rec}) in helium, neon, argon, and krypton for pressures between 0 and 2500 bar. The amplitudes reflect the probability for geminate recombination onto the A/A′ state (see text).

The value of p_{rec} describes the relative importance of the probability for collisional stabilization ($I + I + X \rightarrow I_2^* + X$) versus diffusional separation of the encounter pair. The constant k_{rec}^g (not to be confused with k_{rec}) is taken as the product of the limiting third-order rate coefficient for the nongeminate recombination of iodine at low pressures[26] and the solvent concentration: $d[I_2^*]/dt = k[I]^2[X] = k_{rec}^g[I]^2$. Typical values for the geminate recombination rate are $k_{rec}^g = 5.2 \times 10^6$ m^3 mol^{-1} s^{-1} in helium at 100 bar, 1.6×10^8 m^3 mol^{-1} s^{-1} in argon at 2500 bar, or 8.4×10^7 m^3 mol^{-1} s^{-1} in krypton at 400 bar. The diffusion coefficient for iodine atoms is denoted by D. The probability p_{rec} increases toward unity with increasing pressure since the solvent concentration increases and k_{rec}^g follows; the diffusion coefficient is inversely proportional to the density. In contrast, in the low pressure limit, $k_{rec}^g \rightarrow 0$ and p_{rec} goes to zero.

The total quantum yield for geminate recombination is then obtained as

$$\phi_{rec} = (R_c/r_0)p_{rec} \tag{28}$$

and can be seen as the product of the probability for staying within the solvent cage during the initial separation process and the recombination probability. In the limiting case of low pressures ($p \rightarrow 0$) $D \rightarrow \infty$ and $k_{rec}^g \rightarrow 0$ so that $\phi_{rec} \rightarrow 0$. At high pressures ($p \rightarrow \infty$) $D \rightarrow 0$ so that ϕ_{rec} tends toward unity. As an example, we consider three cases. In helium at 100 bar, $R = 4.9$ Å, $r_0 = 43$ Å, $D = 5 \times 10^{-7}$ m^2/s, and $\phi_{rec} = 3 \times 10^{-4}$; in argon at 2000 bar, $R = 5.5$ Å, $r_0 = 6$ Å, $D = 8 \times 10^{-9}$ m^2/s, and $\phi_{rec} = 0.6$; and in krypton at 400 bar, $R = 5.6$ Å, $r_0 = 8$ Å, $D = 1 \times 10^{-8}$ m^2/s, and $\phi_{rec} = 0.4$. Figure 19 shows a comparison of pressure- and solvent-dependent geminate recombination yields ϕ_{rec} obtained from eq 28 to the experimental results. The predictions of the (parameter-free) OST model are in reasonable agreement with the experimental results.

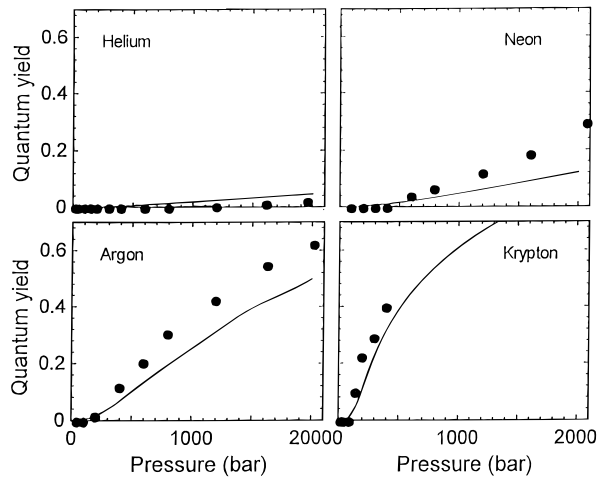

Figure 20. Comparison of experimentally determined quantum yields for geminate recombination with theoretical values from the diffusion-based model (see text). Quantum yields have been obtained by normalization of the recombination amplitude a_{rec} to the known experimental value for the caging yield in krypton at 400 bar of $\phi_{rec} = 0.4$, as discussed in the text.

The model shows the same general pressure dependence as observed experimentally. Above a certain threshold pressure (which decreases with increasing solvent mass), a linear increase of ϕ_{rec} with pressure is observed, and at high pressures ϕ_{rec} approaches asymptotically its limiting value of unity.

The diffusion-based model provides a simple picture that is helpful for a qualitative understanding of the observed solvent- and pressure dependence on the geminate recombination yields. In the limit of very high pressures (not yet reached in our experiments) or in large argon clusters or matrices, iodine is imprisoned in a "perfectly" rigid solvent cage. The probability for "cage breakout" becomes negligibly small, and the recombination dynamics is entirely dominated by the ultrafast recombination within the rigid solvent cage. At the highest argon pressures of the present study, the structure of the first solvent shell is distinctly softer. A finite probability for "cage breakout" exists, and this probability is crucial for the recombination yield and dynamics. While most of the dissociating atoms remain imprisoned within the first solvent shell and recombine within about 1 ps, some of the atoms penetrate the not perfectly rigid cage wall. Once outside the solvent cage, the atomic fragments start a diffusive motion through the solvent and might eventually "meet" again inside the cage. Then again, there will be a finite probability for recombination or diffusional separation.

The recombination dynamics of those atom pairs which are able to leave the solvent cage are determined by the diffusive motion through the solvent and occurs on a distinctly longer time scale than the "direct" in-cage recombination. This will be discussed in full detail in the accompanying paper.[4] As the pressure is lowered, the rigidity of the solvent cage decreases, and the probability for "cage breakout" increases. This lowers the probability for direct "in-cage" recombination. The rate for diffusional separation increases, and the rate for collisional stabilization decreases. This means that a lowering of the solvent pressure also decreases the probability for diffusive geminate recombination. Both effects lead to the observed strong pressure effect on the overall geminate recombination yield.

The above model suggests that the solvent effect on the recombination yield at a given pressure can be attributed to three factors: a change in (a) the initial separation r_0/R, (b) the collisional stabilization efficiency k_{rec}^{g}, and (c) the rate for diffusive separation $4\pi RDN_A$. Though each one of the three factors is only slightly affected by solvent variation, the overall effect on the quantum yield is large. These three factors describe the change in the rigidity of the solvent cage and the probability for the atomic fragments to break through the solvent wall with increasing solvent mass. Although the diffusion model provides accurate predictions of the quantum yields, the recombination dynamics are less well described. A model which treats the solvent as a continuum is less likely to describe the ultrafast direct "in-cage" recombination, especially in the limit of high pressures and rigid solvent cages. As described in ref 5 and in the accompanying paper, molecular dynamics simulations provide a detailed picture of the microscopic forces.

IV. Summary and Conclusion

In this paper, the dissociation and recombination dynamics of a prototype diatomic solute (iodine) in different rare-gas solvents at different densities have been studied, covering the transition region from the gas to the liquid-phase density. With femtosecond time resolution, we are able to examine the elementary processes as the solute−solvent collision time reaches the time scale of the solute nuclear motion. The processes studied are (i) the dephasing of the coherent vibrational wave packet motion within the B state, (ii) the collision-induced B state predissociation; (iii) the geminate recombination of dissociating atomic fragments, and (iv) the relaxation of the vibrationally excited, newly formed iodine molecules on the A/A′ state.

In helium and neon, the coherent wave packet motion persists for many picoseconds, even at pressures of 2000 bar. Surprisingly, the damping of the phase coherence of the vibrational motion in helium and neon solvents appears to be only slightly affected when the pressure is raised from 100 to 2000 bar. At low pressures, vibration−rotation coupling is important to the dephasing mechanism. Due to a motional narrowing effect, the rate of dephasing by vibration−rotation coupling decreases with pressure, so that this mechanism becomes less important. In the high-pressure limit of this study, vibrational dephasing is dominated by the collisional dynamics of the solvent-induced B state predissociation and vibrational relaxation; the maximum value is lower by a factor of 5 than that reported for liquid hexane.

The solvent-induced perturbations were probed by measuring the density dependence of the mean wave packet frequency. The shift of 2−3 cm^{-1}/kbar in He and Ne and ∼7 cm^{-1}/kbar in Ar are significantly larger than that expected from the solvent shift model, indicating *coherent* vibrational energy relaxation. MD simulations in the accompanying paper elucidate the different forces involved.

In all solvents, the collision-induced predissociation rates increase nearly linearly with density and reach 1.05 ps^{-1} in argon at 2500 bar. This proportionality between rates and density indicates the applicability of isolated binary collision models to the dissociation dynamics in high-pressure rare gases. The rate can be expressed as a product of the binary collision frequency between iodine and the rare-gas atoms and a pressure-independent reaction probability per collision. The dependence of the reaction probability on the solvent properties can be understood in terms of a theoretical model based on a Fermi Golden Rule approach to the predissociation rate. Care must be taken in extending the results of this model to predissociation rates in liquid molecular solvents as the concept of a collision time is less defined. It appears that the low probability for dissociation per collision (∼0.1) is the key to the validity of the binary collision model. The predissociation process includes

vibrational relaxation, and MD simulations give the time scales (accompanying paper). Apkarian's group has recently studied I_2 in CCl_4 at room temperature and showed 50% predissociation per vibrational period as opposed to ~3% in solid Kr.[146]

At high solvent densities, a significant fraction of the dissociating atomic fragments geminately recombine to form new molecules on either the A/A′ state or the ground state. Experiments with UV probe pulses provide information on the relative yield for recombination on the A/A′ states as well as on the dynamics of recombination and subsequent vibrational relaxation. Through variation of the solvent density, the yield for geminate recombination is varied from 0 at low pressures to 0.6 in argon at 2500 bar. At a given pressure, the geminate recombination yield increases drastically with increasing solvent size. A comparison of the experimental results to a diffusion-based theoretical model indicates that the change in the rigidity of the solvent cage with increasing solvent size is crucial for this pronounced effect. The critical factors are (1) the probability for cage breakout during the separation and energy transfer to the solvent, which follows the initial dissociation, (2) the efficiency of the solvent for collisional stabilization of iodine encounter pairs inside the cage, and (3) and the probability for diffusional separation of the encounter pairs. The findings are entirely consistent with earlier work on clusters[5,59] where caging was found to be prompt and coherent (~0.7 ps) in the rigid solvent structure.

Rare gases are ideal solvents for a theoretical treatment of the dissociation and caging dynamics as the potential energy surfaces of the iodine valence states are only slightly perturbed, and information on the solvent influence on the ion-pair states is available. MD simulations are detailed in the accompanying third paper. Studies in more complex solvents are a natural extension of this work.

Acknowledgment. This work was supported by the National Science Foundation. Ch.L. gratefully acknowledges a postdoctoral fellowship by the Deutsche Forschungsgemeinschaft. We thank Mr. Chris Hyland for his help in some of these studies.

Appendix. Densities and Diffusion Coefficients

In this appendix, we describe briefly how the pressure-dependent thermophysical properties of rare gases, which were needed in order to calculate quantum yields for atomic recombination of iodine using eq 28, were determined or, whenever necessary, estimated.

Accurate experimental determinations of the density of rare gases as a function of pressure and temperature in the pressure range from 0 to 2000 bar are available in the literature for helium,[124,125] neon,[126] argon,[127] and krypton.[128] To obtain values at 293 K, we interpolated linearly between the values quoted for the next lower and higher temperature. The interpolated density values as a function of pressure were fit to a polynomial of degree less than or equal to 10. In all cases the error of the extrapolated density values is expected to be less than 1%.

Experimental values of the viscosity at high pressures of helium,[129,130] neon,[131,132] argon,[133−137] and krypton[138−140] can also be found in the literature for several temperatures. These values have again been extrapolated to 293 K and then fitted to polynomials. The error in the extrapolated viscosities is believed to be less than 2%.

Diffusion coefficients for iodine atoms in rare gases could not be found in the literature. Pressure-dependent studies of diffusion coefficients in compressed gases are rare. Diffusion coefficients for krypton-85 in helium, argon, and krypton at 308 K in the pressure range from 1 to 420 bar are given in ref 141. In order to extrapolate diffusion coefficients for iodine atoms in the pressure range from 0 to 2000 bar, we used an empirical relation between diffusion coefficient and viscosity proposed by Troe and co-workers.[142] This relation, which allows for an interpolation between diffusion coefficients obtained using the kinetic theory of dilute gases[143] at low pressures and the Stokes−Einstein relationship[144] at liquid densities, is given by

$$\frac{kT}{\eta_1 D_{12}}(p) = \left(\frac{kT}{\eta_1 D_{12}}\right)^{\infty}\left\{1 - \exp\left(-\frac{(kT/\eta_1 D_{12})^0(p)}{(kT/\eta_1 D_{12})^{\infty}}\right)\right\} \quad \text{(A.1)}$$

where k denotes the Boltzmann constant, T the temperature, η_1 the experimentally known viscosity of the solvent, and D_{12} the binary diffusion coefficient of molecule 2 in solvent 1 at the pressure p. The subscripts 0 and ∞ denote the high- and low-pressure limits of $kT/\eta_1 D_{12}$, respectively. In the high-pressure limit the Stokes−Einstein relationship applies, and $kT/\eta_1 D_{12}$ is given by

$$\lim_{p\to\infty} \frac{kT}{\eta_1 D_{12}} = \left(\frac{kT}{\eta_1 D_{12}}\right)^{\infty} = 3\pi d_2 \quad \text{(A.2)}$$

with d_2 being the (Lennard-Jones) diameter of the molecule 2 (for iodine atoms $d_2 = 4.320$ Å).[145]

In the low-pressure limit, kinetic gas theory is applicable, and $kT/\eta_1 D_{12}$ becomes proportional to the solvent density ρ:

$$\lim_{p\to 0} \frac{kT}{\eta_1 D_{12}}(p) = \left(\frac{kT}{\eta_1 D_{12}}\right)^{0}(p) = \left(\frac{kT}{\eta_1 D_{12}}\right)^{0}(1\text{ bar})\frac{\rho(p)}{\rho(1\text{ bar})} \quad \text{(A.3)}$$

Since both the density and viscosity are known as a function of pressure, the only unknown is the binary diffusion coefficient $D_{1,I}$ ($p = 1$ bar, $T = 293$ K) for iodine atoms in rare gases. $D_{1,I}$ has been extrapolated from the experimentally known $D_{1,Kr}$ ($p = 1$ bar, $T = 308$ K) using the kinetic gas theory equation

$$D_{12}^0 = \frac{3}{8}\frac{\sqrt{\pi kT/2\mu_{12}}}{\pi d_{12}^2 \Omega_{12}^{(1,1)*}}\frac{1}{\rho_1 N_A} \quad \text{(A.4)}$$

and Lennard-Jones potential parameters from ref 145. μ_{12} denotes the reduced mass, $m_1 m_2/(m_1 + m_2)$, $d_{12} = (d_1 + d_2)/2$ is the relative Lennard-Jones collision diameter, N_A is Avogadro's number, and $\Omega_{12}^{(1,1)*}$ is the reduced (Lennard-Jones) collision integral.

References and Notes

(1) Lienau, Ch.; Williamson, J. C.; Zewail, A. H. *Chem. Phys. Lett.* **1993**, *213*, 289.
(2) Lienau, Ch.; Zewail, A. H. *Chem. Phys. Lett.* **1994**, *218*, 224.
(3) Lienau, Ch.; Zewail, A. H. *J. Chim. Phys.* **1995**, *92*, 566.
(4) Materny, A.; Lienau, Ch.; Zewail, A. H. *J. Phys. Chem.* **1996**, *100*, 18650.
(5) Wang, J.-K.; Liu, Q.; Zewail, A. H. *J. Phys. Chem.* **1995**, *99*, 11309. Liu, Q.; Wang, J.-K.; Zewail, A. H. *J. Phys. Chem.* **1995**, *99*, 11321.
(6) Gerstenkorn, S.; Luc, P. *J. Phys. (Paris)* **1985**, *46*, 867.
(7) Zheng, X.; Fei, S.; Heaven, M. C.; Tellinghuisen, J. *J. Chem. Phys.* **1992**, *96*, 4877.
(8) Visnawathan, K. S.; Sur, A.; Tellinghuisen, J. *J. Mol. Spectrosc.* **1981**, *86*, 393.
(9) Tellinghuisen, J. *J. Chem. Phys.* **1985**, *82*, 4012.
(10) Churassy, S.; Martin, F.; Bacis, R.; Vergès, J.; Field, R. W. *J. Chem. Phys.* **1981**, *75*, 4863.
(11) Martin, F.; Churassy, S.; Bacis, R.; Vergès, J.; Field, R. W. *J. Chem. Phys.* **1983**, *79*, 3725.
(12) Zheng, X.; Fei, S.; Heaven, M. C. *J. Mol. Spectrosc.* **1991**, *149*, 399.
(13) Bartels, M.; Donovan, R. J.; Holmes, A. J.; Langridge-Smith, P.; MacDonald, M. A.; Ridley, T. *J. Chem. Phys.* **1989**, *91*, 7355.

(14) Brand, J. C. D.; Hoy, A. R.; Kalkar, A. K.; Yamashita, A. B. *J. Mol. Spectrosc.* **1982**, *95*, 350.
(15) Hickmann, J. S.; de Olivera, C. R. M.; Francke, R. E. *J. Mol. Spectrosc.* **1982**, *95*, 350.
(16) Bowman, R. M.; Dantus, M.; Zewail, A. H. *Chem. Phys. Lett.* **1989**, *161*, 297.
(17) Dantus, M.; Bowman, R. M.; Zewail, A. H. *Nature* **1990**, *343*, 737.
(18) Gruebele, M.; Zewail, A. H. *J. Chem. Phys.* **1993**, *98*, 883.
(19) Bernstein, R. B.; Zewail, A. H. *Chem. Phys. Lett.* **1990**, *170*, 321.
(20) Zewail, A. H.; Dantus, M.; Bowman, R. M.; Mokthari, A. *J. Photochem. Photobiol. A* **1992**, *62*, 301.
(21) Yan, Y.; Whitnell, R. M.; Wilson, K. R.; Zewail, A. H. *Chem. Phys. Lett.* **1992**, *193*, 402.
(22) Schroeder, J.; Troe, J. *Annu. Rev. Phys. Chem.* **1987,** *38*, 163.
(23) Troe, J. *J. Phys. Chem.* **1986**, *90*, 357.
(24) Hippler, H.; Schubert, V.; Troe, J. *J. Chem. Phys.* **1984**, *81*, 3921.
(25) Luther, K.; Troe, J. *Chem. Phys. Lett.* **1974**, *24*, 85.
(26) Hippler, H.; Luther, K.; Troe, J. *Ber. Bunsen-Ges. Phys. Chem.* **1973**, *77*, 1104.
(27) Dutoit, J. C.; Zellweger, J. M.; van den Bergh, H. *J. Chem. Phys.* **1983**, *78*, 1825.
(28) Zellweger, J. M.; van den Bergh, H. *J. Chem. Phys.* **1980**, *72*, 5405.
(29) Otto, B.; Schroeder, J.; Troe, J. *J. Chem. Phys.* **1984**, *81*, 202.
(30) Franck, J.; Rabinowitch, E. *Trans. Faraday Soc.* **1930**, *30*, 120.
(31) Rabinowitch, E.; Wood, W. C. *Trans. Faraday Soc.* **1936,** *32*, 547, 1381.
(32) Zimmerman, J.; Noyes, R. M. *J. Chem. Phys.* **1950,** *18*, 658.
(33) Meadows, L. F.; Noyes, R. M. *J. Am. Chem. Soc.* **1960,** *82*, 1872.
(34) Bunker, D. L.; Davidson, N. *J. Am. Chem. Soc.* **1958**, *80*, 5090.
(35) Porter, G.; Smith, J. A. *Proc. R. Soc. London, Ser. A* **1961**, *261*, 28.
(36) Booth, D.; Noyes, R. M. *J. Am. Chem. Soc.* **1960,** *82*, 1868.
(37) Chuang, T. J.; Hoffmann, G. W.; Eisenthal, K. B. *Chem. Phys. Lett.* **1974**, *25*, 201.
(38) Nesbitt, D.; Hynes, J. T. *J. Chem. Phys.* **1982**, *77*, 2130.
(39) Bado, P.; Berens, P. H.; Wilson, K. R. *Proc. Soc. Photo-Opt. Instrum. Eng.* **1982**, *332*, 230.
(40) Bunker, D. L.; Jacobsen, B. S. *J. Am. Chem. Soc.* **1972**, *94*, 1843.
(41) Murrell, J. N.; Stace, A. J.; Dammel, R. *J. Chem. Soc., Faraday Trans. 2* **1978**, *74*, 1532.
(42) Lipkus, A. H.; Buff, F. P.; Sceats, M. G. *J. Chem. Phys.* **1983**, *79*, 4830.
(43) Kelley, D. F.; Abul-Haj, N. A.; Jang, D. J. *J. Chem. Phys*. **1984**, *80*, 4105.
(44) Abul-Haj, N. A.; Kelley, D. F. *Chem. Phys. Lett.* **1985**, *119*, 182.
(45) Abul-Haj, N. A.; Kelley, D. F. *J. Chem. Phys.* **1986**, *84*, 1335.
(46) Bado, P.; Wilson, K. R. *J. Phys. Chem.* **1984**, *88*, 655.
(47) Bado, P.; Dupuy, C.; Magde, D.; Wilson, K. R. *J. Chem. Phys.* **1984**, *80*, 5531.
(48) Harris, A. L.; Brown, J. K.; Harris, C. B. *Annu. Rev. Phys. Chem.* **1988**, *39*, 341.
(49) Berg, M.; Harris, A. L.; Harris, C. B. *Phys. Rev. Lett.* **1985**, *54*, 951.
(50) Berg, M.; Harris, A. L.; Harris, C. B. *J. Chem. Phys.* **1986**, *84*, 788.
(51) Smith, D. E.; Harris, C. B. *J. Chem. Phys.* **1987**, *87*, 2709.
(52) Paige, M. E.; Harris, C. B. *J. Chem. Phys.* **1990**, *93*, 1481.
(53) Paige, M. E.; Harris, C. B. *Chem. Phys.* **1990**, *149*, 37.
(54) Xu, J.; Yu, S.-C.; Lingle, R.; Zhu, H.; Hopkins, J. B. *J. Chem. Phys.* **1991**, *95*, 2445.
(55) Scherer, N. F.; Ziegler, L. D.; Fleming, G. R. *J. Chem. Phys.* **1992**, *96*, 5544.
(56) Scherer, N. F.; Jonas, D. M.; Fleming, G. R. *J. Chem. Phys.* **1993**, *99*, 153.
(57) Sension, R.; Strauss, H. *J. Chem. Phys.* **1986**, *85*, 3791.
(58) Xu, J.; Schwentner, N.; Chergui, M. *J. Chem. Phys.* **1994**, *101*, 7381. Xu, J.; Schwentner, N.; Henning, S.; Chergui, M. *J. Chim. Phys. Phys.-Chim. Biol*. **1995**, *92*, 541.
(59) Liu, Q.; Wang, J.-K.; Zewail, A. H. *Nature* **1993**, *364*, 427. Potter, E. D.; Liu, Q.; Zewail, A. H. *Chem. Phys. Lett.* **1992**, *200*, 605.
(60) Zadoyan, R.; Li, Z.; Ashjian, P.; Martens, C. C.; Apkarian, V. A. *Chem. Phys. Lett.* **1994**, *218*, 504; Zadoyan, R.; Li, Z.; Martens, C. C.; Apkarian, V. A. *J. Chem. Phys.* **1994**, *101*, 6648. Li, Z.; Zadoyan, R.; Apkarian, V. A.; Martens, C. C. *J. Phys. Chem.* **1995**, *99*, 7453.
(61) Martens, C. C. In *Femtochemistry: Ultrafast Chemical and Physical Processes in Molecular Systems*; Chergui, M., Ed.; World Scientific: Singapore, 1996, and references therein.
(62) Li, Z.; Fang, J.-Y.; Martens, C. C. *J. Chem. Phys.* **1996**, *104*, 6919.
(63) The "packing fraction" is defined as the product of solvent density ρ (mol/L) and the molar volume V_0 of the solvent atoms, which is assumed to be given as $V_0 = {}^1/_6\pi d^3 N_A$, with d being the Lennard-Jones diameter and N_A Avogadro's number. Lennard-Jones diameters: He, 2.576 Å; Ne, 2.789 Å; Ar, 3.418 Å; Kr, 3.6 Å; I_2, 4.982 Å.
(64) A hard-sphere collision frequency $z_{I_2-RG} = d^2_{I_2-RG}(8\pi kT/\mu_{I_2-RG})^{1/2} N_A \rho$ is assumed, with d_{I_2-RG} being the Lennard-Jones diameter (m), μ_{I_2-RG} the reduced mass (kg), k Boltzmann's constant, T the temperature (K), N_A Avogadro's number, and ρ the density (mol/L).
(65) Tellinghuisen, J. *J. Chem. Phys.* **1973**, *58*, 2821.
(66) Holmes, A. J.; Lawley, K. P.; Ridley, T.; Donovan, R. J.; Langridge-Smith, P. R. *J. Chem. Soc., Faraday Trans.* **1991**, *87*, 15.
(67) Heemann, U.; Knöckel, H.; Tiemann, E. *Chem. Phys. Lett.* **1982**, *90*, 350.
(68) Brand, J. C. D.; et al. *J. Mol. Spectrosc.* **1982**, *95*, 350 and references therein (ref 14).
(69) Brand, J. C. D.; Hoy, A. R. *Can. J. Phys.* **1982**, *60*, 1209.
(70) Martin, M.; Fotakis, C.; Donovan, R. J.; Shaw, M. J. *Nuovo Cimento* **1981**, *63*, 300.
(71) Fei, S.; Zheng, X.; Heaven, M. C.; Tellinghuisen, J. *J. Chem. Phys.* **1992**, *97*, 6057.
(72) Bell, R. P. *Trans. Faraday Soc.* **1931**, *27*, 797.
(73) Onsager, L. *J. Am. Chem. Soc.* **1936**, *58*, 1486.
(74) Böttcher, C. J. F. *Theory of Electric Polarization*; Elsevier: Amsterdam, 1973.
(75) Vidal, D.; Lallemand, M. *J. Chem. Phys.* **1976**, *64*, 4293.
(76) Macler, M.; Heaven, M. C. *Chem. Phys.* **1991**, *151*, 219.
(77) Hoy, A. R.; Taylor, A. W. *J. Mol. Spectrosc.* **1987**, *126*, 484.
(78) Guy, A.; Visnawathan, K. S.; Sur, A.; Tellinghuisen, J. *Chem. Phys. Lett.* **1980**, *73*, 582.
(79) Benesi, H. A.; Hildebrand, J. H. *J. Am. Chem. Soc.* **1949**, *72*, 2703.
(80) Mulliken, R. S. *J. Am. Chem. Soc.* **1950**, *72*, 600; **1952**, *74*, 811.
(81) Cheng, P.-Y.; Zhong, D.; Zewail, A. H. *J. Chem. Phys.* **1995**, *103*, 5153; *Chem. Phys. Lett.* **1995**, *242*, 369; *J. Chem Phys*., in press.
(82) Lenderink, E.; Duppen, K.; Wiersma, D. A. *Chem. Phys. Lett.* **1993**, *211*, 503.
(83) Kiefer, W.; Bernstein, H. J. *J. Raman Spectrosc.* **1973**, *1*, 417.
(84) Ben-Amotz. D.; Herschbach, D. R. *J. Phys. Chem.* **1993**, *97*, 2295 and references therein for the original work by D. Buckingham and others.
(85) Schweizer, K. S.; Chandler, D. S. *J. Chem. Phys.* **1982**, *76*, 2296.
(86) Ben-Amotz, D.; Lee, M. R.; Cho, S. Y.; List, D. L. *J. Chem. Phys.* **1992**, *96*, 8781.
(87) Pugliano, N.; Szarka, A. Z.; Hochstrasser, R. M. *J. Chem. Phys.* **1996**, *104*, 5062. Fleming, G. R.; Joo, T.; Cho, M. *Adv. Chem. Phys*., in press.
(88) Banin, U.; Ruhmann, S. *J. Chem. Phys.* **1993**, *98*, 4391. Banin, U.; Kosloff, R.; Ruhmann, S. *Chem. Phys.* **1994**, *183*, 289.
(89) Shelby, R. M.; Harris, C. B.; Cornelius, P. A. *J. Chem. Phys.* **1979**, *70*, 34.
(90) Schweizer, K. S.; Chandler, D. *J. Chem. Phys.* **1982**, *76*, 2296.
(91) Oxtoby, D. W. *Annu. Rev. Phys. Chem.* **1981**, *32*, 79.
(92) Oxtoby, D. W. *Adv. Chem. Phys.* **1979**, *40*, 1; **1981**, *47*, 487.
(93) Fischer, S. F.; Laubereau, A. *Chem. Phys. Lett.* **1975**, *35*, 6.
(94) Neumann, M.; Tabisz, G. C. *Mol. Phys.* **1982**, *47*, 849.
(95) Robert, D.; Bonamy, J.; Sala, J. P.; Levi, G.; Marsault-Herail, F. *Chem. Phys.* **1985**, *99*, 303.
(96) Aechtner, P.; Laubereau, A. *Chem. Phys.* **1991**, *151*, 419.
(97) Neuman, M.; Tabisz, G. C. *Mol. Phys.* **1982**, *47*, 861.
(98) Bizot, P.; Echargui, M. A.; Marsault, J. P.; Marsault-Herail, F. *Mol. Phys.* **1993**, *79*, 489.
(99) Anderson, P. W. *J. Phys. Soc. Jpn.* **1954**, *9*, 316.
(100) Kubo, R. *J. Phys. Soc. Jpn.* **1954**, *9*, 935.
(101) Brueck, S. R. J. *Chem. Phys. Lett.* **1977**, *50*, 516.
(102) Steinfeld, J. I. *Acc. Chem. Res.* **1970**, *3*, 313.
(103) Chesnoy, J.; Weis, J. J. *J. Chem. Phys*. **1986**, *84*, 5378.
(104) In order to avoid the ambiguity sometimes appearing in the literature, where σ is somtimes taken to be a cross section (m^2) and sometimes to be a distance (m), we denote the Lennard-Jones diameter by d. The following parameters have been used: Lennard-Jones diameters: He, 2.576 Å; Ne, 2.789 Å; Ar, 3.418 Å; Kr, 3.6 Å; I2, 4.982 Å; *n*-hexane, 5.909 Å.
(105) Steinfeld, J. I. *J. Chem. Phys*. **1966**, *44*, 2740.
(106) Capelle, G. A.; Broida, H. P. *J. Chem. Phys.* **1973**, *58*, 4212.
(107) Selwyn, J. E.; Steinfeld, J. I. *Chem. Phys. Lett.* **1969**, *4*, 217.
(108) Margenau, H. *Rev. Mod. Phys.* **1939**, *11*, 1.
(109) The following parameters have been used: Lennard-Jones diameters: He, 2.576 Å; Ne, 2.789 Å; Ar, 3.418 Å; Kr, 3.6 Å; I_2, 4.982 Å; *n*-hexane, 5.909 Å. Polarizabilities (10^{-30} m^3): He, 0.2050; Ne, 0.3956; Ar, 1.6411; Kr, 2.4844; hexane, 11.78. Ionization potentials (eV): He, 24.587; Ne, 21.564; Ar, 15.795; Kr, 13.999; hexane, 10.18.
(110) We assume a laser pulse energy of 10 μJ, or 3×10^{13} photons per pulse at 620 nm, a beam diameter of 2 mm, and an optical path length of 6 mm. The iodine vapor pressure at room temperature is about 0.3 mbar, corresponding to an iodine concentration of 1.4×10^{-5} mol L^{-1}. For an extinction coefficient of 78 L mol^{-1} cm^{-1}, Lambert−Beer's law gives a total absorption of the laser pulse of 0.15%. This corresponds to 4.5×10^{10} photoexcited iodine molecules or, correspondingly, a concentration of 4×10^{-9} mol L^{-1}.

(111) Recombination amplitudes larger than one do not correspond to quantum yields for geminate recombination larger than one. At 310 nm the A/A′ state extinction coefficient (≅12 000 L mol^{-1} cm^{-1}) is significantly larger than that of the B state.

(112) Bado, P.; Berens, P. H.; Bergsma, J. P.; Wilson, S. B.; Wilson, K. R. In *Picosecond Phenomena III*; Eisenthal, K. B., Hochstrasser, R. M., Kaiser, W., Laubereau, A., Ed.; Springer: Berlin, 1982.

(113) Bunker, D. L.; Jacobson, B. S. *J. Am. Chem. Soc.* **1973**, *94*, 1843.

(114) Murrell, J. N.; Stace, A. J.; Dammel, R. *J. Chem. Soc. Faraday Trans. 2* **1978**, *74*, 1532.

(115) Stace, A. J. *J. Chem. Soc. Faraday Trans. 2* **1981**, *77*, 2105.

(116) Lipkus, A. H.; Buff, F. B.; Sceats, M. G. *J. Chem. Phys.* **1983**, *79*, 4830.

(117) Adelman, S. A. *J. Chem. Phys.* **1980**, *73*, 3145.

(118) Adelman, S. A. *Adv. Chem. Phys.* **1980**, *44*, 143.

(119) Brooks, C. L.; Balk, M. W.; Adelman, S. A. *J. Chem. Phys.* **1983**, *79*, 784, 804.

(120) Noyes, R. M. *Z. Elektrochem.* **1960**, *64*, 153; *Prog. React. Kinet.* **1961**, *1*, 131.

(121) Schulten, Z.; Schulten, K. *J. Chem. Phys.* **1977**, *66*, 4616.

(122) Tachiya, M. *J. Chem. Phys.* **1978**, *69*, 2375.

(123) Razi Naqvi, K.; Mork, K. J.; Waldenstrøm, S. *J. Phys. Chem.* **1980**, *84*, 1315.

(124) McCarty, R. D. *J. Phys. Chem. Ref. Data* **1973**, *2*, 923.

(125) ten Seldam, C. A.; Biswas, S. N. *J. Chem. Phys.* **1992**, *96*, 6163.

(126) Michels, A.; Wassenaar, T.; Louwerse, P. *Physica* **1960**, *26*, 539.

(127) Stewart, R. B.; Jacobsen, R. T. *J. Phys. Chem. Ref. Data* **1989**, *18*, 639.

(128) Trappeniers, N. J.; Wassenaar, T.; Wolkers, G. J. *Physica* **1966**, *32*, 1503.

(129) Vermesse, J.; Vidal, D. *C. R. Seances Acad. Sci., Ser. B* **1976**, *282*, 5.

(130) Kao, J. F. F.; Kobayashi, R. *J. Chem. Phys.* **1967**, *47*, 2836.

(131) Vermesse, J.; Vidal, D. *C. R. Seances Acad. Sci., Ser. B* **1975**, *280*, 56.

(132) Trappeniers, N. J.; Botzen, A.; van den Berg, H. R.; van Oosten, J. *Physica* **1964**, *30*, 985.

(133) Hanley, H. J. M.; McCarty, R. D.; Haynes, W. M. *J. Phys. Chem. Ref. Data* **1974**, *3* 979.

(134) van der Gulik, P. S.; Trappeniers, N. J. *Physica* **1986**, *135 A*, 1.

(135) Trappeniers, N. J.; van der Gulik, P. S.; van den Hooff, H. *Chem. Phys. Lett.* **1980**, *70*, 438.

(136) Vermesse, J.; Vidal, D. *C. R. Seances Acad. Sci., Ser. B* **1973**, *277*, 191.

(137) Michels, A.; Botzen, A.; Schurman, W. *Physica* **1954**, *20*, 1141.

(138) Hanley, H. J. M.; McCarty, R. D.; Haynes, W. M. *J. Phys. Chem. Ref. Data*, **1974**, *3*, 979.

(139) Vermesse, J.; Provansal, M.; Brielles, J. *Physica* **1978**, *92A*, 282.

(140) Trappeniers, N. J.; Botzen, A.; van Oosten, J.; van den Berg, H. R. *Physica* **1965**, *31*, 945.

(141) Durbin, L.; Kobayashi, R. *J. Chem. Phys.* **1962**, *37*, 1642.

(142) Hippler, H.; Schubert, V.; Troe, J. *Ber. Bunsen-Ges. Phys. Chem.* **1985**, *89*, 760.

(143) Hirschfelder, J. O.; Curtiss, C. F.; Bird, R. B. *Molecular Theory of Gases and Liquids*, John Wiley: New York, 1954.

(144) Einstein, A. *Z. Elektrochem.* **1907**, *13*, 41; **1908**, *14*, 235.

(145) Shevla, R. A. NASA Technical Report R. 132, Cleveland, OH, 1962.

(146) Zadoyan, R.; Sterling, M.; Apkarian, V. A. *J. Chem. Soc., Faraday Trans.* **1996**, *92* (11), 1821; private communication.

JP962430A